A Lattice-Gas Model of Microemulsions

Bruce M. Boghosian,
Center for Computational Science, Boston University,
3 Cummington Street, Boston,Massachusetts 02215, U.S.A.
Peter V. Coveney
Schlumberger Cambridge Research,
High Cross, Madingley Road, Cambridge CB3 0EL, UK.
and
Andrew N. Emerton
Theoretical Physics, Department of Physics, University of Oxford
1 Keble Road, Oxford OX1 3NP, UK

(July 10, 1995)

We develop a lattice gas model for the nonequilibrium dynamics of microemulsions. Our model is based on the immiscible lattice gas of Rothman and Keller, which we reformulate using a microscopic, particulate description so as to permit generalisation to more complicated interactions, and on the prescription of Chan and Liang for introducing such interparticle interactions into lattice gas dynamics. We present the results of simulations to demonstrate that our model exhibits the correct phenomenology, and we contrast it with both equilibrium lattice models of microemulsions, and to other lattice gas models.

I. INTRODUCTION

It is well known that oil and water do not mix, and yet, with the addition of *amphiphile* (or *surfactant*) to such systems, one can observe the formation of a wealth of complex structures. For a general review see Gelbart *et. al.* (1993). The complex structures themselves arise as a result of the particular physical and chemical properties of the amphiphile, the most important of these being the polar nature of the molecules, typically, an ionic head which is attracted to water, and a hydrocarbon tail which prefers oil. Consequently there is a strong energy preference for the surfactant molecules to be absorbed at, and thereby to cause the formation of, oil-water interfaces. The aforementioned structures occur in both binary (surfactant and water or oil) and ternary systems; they are in general strongly dependent on the relative quantity and nature of the surfactant molecules present (whether the amphiphile has an ionic or non-ionic nature, the size of the hydrophobic tail, and so on), and on the temperature of the system. The equilibrium properties of these complex structures are conveniently described by the numerous phase diagrams that have been obtained from experimental investigation (Kahlweit *et. al* 1987). The *microemulsion* phase itself occurs only within a certain region of the ternary phase space. It is of particular industrial interest because of the very low surface tensions that exist between the so called "middle phase" microemulsion and bulk oil and water phases (*cf.* normal bulk oil-water surface tension), see Cazabat *et. al.* (1982). The complex nature and wide industrial application of these systems make them ideal subjects for experimental, theoretical and numerical investigation. Most previous work in this area has been done on the equilibrium phase behaviour (Gompper & Schick 1995) of such self-assembling systems; comparatively little research has been devoted to their nonequilibrium, dynamic properties (Kawakatsu *et. al* 1993). Here we develop a computational technique, with a theoretical basis, that has the ability to simulate self-assembling amphiphilic systems under both equilibrium and nonequilibrium conditions.

Lattice gases have been used as a numerical technique for modelling hydrodynamics since their introduction

in 1986 by Frisch, Hasslacher and Pomeau (Frisch *et al.* 1986) and by Wolfram (Wolfram 1986), who showed that one could simulate the solution of the incompressible Navier-Stokes equations using a class of deterministic lattice gases with discrete Boolean elements. The method was later generalised by Rothman and Keller (Rothman & Keller 1988) to enable the simulation of two immiscible fluids, and we use their model, which has since been investigated with some degree of rigour (see Sec. III), as the basic starting point for ours.

The simulation of the behaviour of three-phase fluids is a complex and challenging area of computational science. Previously, certain lattice-gas models for three immiscible fluids (Gunstensen & Rothman 1991a) have been found to exhibit numerical difficulties, including a very high diffusivity of one fluid into another, very large interfacial fluctuations and limited control over the relative strength of the surface tension coefficients; such problems have encouraged a trend towards the study of simpler lattice-Boltzmann techniques (Gunstensen 1992). Furthermore, the complexity of microemulsion behaviour goes well beyond that of immiscible fluids and so has been out of reach of these types of models until now. In this paper we develop a version of such a model that simulates the nonequilibrium, dynamical properties of amphiphilic systems, and in particular of microemulsions. Note that the use of the basic lattice gas model, in contrast to, for example, molecular dynamics simulations, gives us the ability to investigate the important late-time dynamics of these systems (Kawakatsu *et al.* 1993) in a computationally tractable manner. Also, since lattice-gas models enable the implementation of complex boundary conditions, we can simulate very realistic interface formation and dynamics and investigate such systems under flow and within complex media such as porous rock.

The purpose of the present paper is to define and establish the general validity of our model; we show that our model can reproduce certain known features of these self-assembling amphiphilic systems. we show that our model can reproduce. In Section II we briefly review some of the work that has already been done on the modelling of self-assembling amphiphilic systems. Sections III and IV contain the description and formulation of our model, while the results of simulations we have performed are described in Section V. These two-dimensional (2D) simulations demonstrate the ability of our model to capture the phenomenology of various self-assembling amphiphilic structures in a consistent way, including the propensity for the surfactant molecules to sit in thin layers at oil-water interfaces and the arrest of separation of the immiscible oil-water phases when enough surfactant is present in the system. In Section VII we draw some conclusions from this work.

II. EQUILIBRIUM MODELS OF MICROEMULSIONS

Microemulsion models are characterized by the fundamental length and energy scales on which the system is described. On this basis we can categorise the three principal types of theories that have emerged, namely membrane models, Ginzburg-Landau theories, and microscopic models. For a review of such approaches see Gompper and Schick (Gompper & Schick 1995) and references contained therein.

Membrane theories take as the basic statistical entities sheets of amphiphile, whether monolayer or bilayer, thereby providing a universal description for ternary and binary mixtures. The basic energy scale is that needed to bend the sheet, and the local free energy per unit area is written as an expansion in powers of the local curvature. The membrane approach is most useful for the study of the fluctuations of a single membrane, or of those characterizing a bulk phase whose scaling behaviour is readily obtained.

Ginzburg-Landau theories are described in terms of order parameters, which represent microscopic quantities averaged over extended regions of phase space. The free energy is often simply constructed from symmetry arguments once the choice of order parameters describing the system has been made. The advantage of such theories is that they are simple enough to permit analytic analysis, to easily describe bulk and interfacial properties, and to calculate structure functions of the various phases. Again the mesoscopic length scales of the microemulsion must emerge from the theory, as they are much larger than the input length scales.

The fundamental length scales of microscopic models are molecular ones. The mesoscopic lengths observed in the experimental analysis of such systems (scattering experiments and micrographs) must then be derived from the theory. All such theories to date have attempted to derive generic behaviour and so

2

the distinguishing features of particular amphiphiles and oils are largely ignored. The interactions included are invariably of short range, while the amphiphile molecules are treated either as scalar particles without internal structure or as vectors whose interaction energies depend on how they align with themselves and the other entities in the system. An additional simplification that is often made is to replace the continuum system by a discrete one, which then reduces the model to the form of a general lattice gas. Advantages of this lattice approach include its ability to model both bulk phase and interfacial behaviour. Furthermore, the structure of interfaces, their tensions and associated wetting properties can be observed at the molecular level, while the equilibrium structure of the microemulsion itself can be examined by lattice-based Monte-Carlo simulation techniques. It is worth noting that hybrid models (Kawakatsu & Kawasaki 1990) for the simulation of immiscible binary mixtures with surfactant molecules have been derived; these make use of a combination of time-dependent Ginzburg-Landau theory for the underlying binary fluid and discrete particles with dipolar orientation to describe the surfactant molecules.

Since our model is based on a microscopic treatment of the lattice gas particles, we look in more detail at some of the various microscopic models that have been investigated. There are numerous lattice-based microscopic models, including the three component model of Schick and Shih (1987), where all three components are found on lattice sites and a fairly simple Hamiltonian describes the interactions in the system. This includes a three-particle interaction term that allows the most obvious property of amphiphiles - their tendency to sit between oil and water - to be modelled without having to introduce extra degrees of freedom associated with their directional properties. This type of Hamiltonian can be generalized further with a four-particle interaction term that allows the various structures forming in binary systems, including amphiphilic bilayers, to be modelled (Gompper & Schick 1989).

One much studied lattice model, introduced by Widom (Widom 1984; Widom 1986; Widom & Dawson 1986), again has three species, but in this case the molecules are confined to the *bonds* of a regular lattice. The advantage of this model is that it is exactly equivalent to a spin-$\frac{1}{2}$ Ising model in a magnetic field, with ferromagnetic nearest-neighbour, antiferromagnetic next-nearest-neighbour, and three-spin interactions. The model allows a straightforward representation of many of the observed microemulsion-like structures, and it has the correct pattern of phase equilibria, interface phenomena and interfacial tension (Dawson 1986). There are many more generalisations of both the Widom and the three-component models. One such example is the Alexander model (Stockfish & Wheeler 1988), in which the molecules are not treated symmetrically; oil and water particles are placed on the lattice sites, at which up to two molecules can reside, and amphiphiles on the bonds, which are otherwise empty. As mentioned above, other microscopic models exist which allow the amphiphilic molecules to have orientational degrees of freedom. These are called vector models and generally consist of a simple Hamiltonian for a ternary mixture on a lattice, with an additional Hamiltonian that governs the orientation-dependent interactions. Some of these models allow the vector amphiphile to have a continuous orientational degree of freedom (Gompper & Schick 1989), while others permit the vector amphiphile to point only towards nearest-neighbour sites (Matsen & Sullivan 1990).

In general the phase behaviour and/or phase diagrams obtained from all these models are reasonable, although for the most part they bear little actual resemblence to experimentally derived ones. This is because for the most part they are given as functions of theoretical interaction parameters and what one would really like to see is transitions due to changes in the relative concentration of amphiphile or temperature. It is intended that our model should have the ability to do this. The microscopic approach is also particularly appropriate for the study of self-assembly, in that the amphiphilic molecules are free to form interfaces or micelles as they choose. However, it is important to note that, aside from the hybrid model, all the models introduced above have the ability to model only static, equilibrium phase behaviour. The dynamics of such amphiphilic systems are unattainable by these methods. Another element lacking is any unified approach to binary and ternary systems, for example, there have been few attempts to describe a system as it evolves from a balanced ternary one to a binary one as oil, or water, is withdrawn. The model we present in this paper aims to correct many of the above mentioned deficiences.

III. IMMISCIBLE LATTICE GASES

Lattice gases for the simulation of the flow of immiscible Navier-Stokes fluids were first introduced by Rothman and Keller in 1988 (Rothman & Keller 1988). They generalised the work of FHP to include new degrees of freedom and collision rules that gave rise to immiscible two-phase flow. The Rothman-Keller model can be described by supposing that the lattice gas particles are of two or more different *colours*, to denote the two immiscible species. They then defined the local colour flux of the particles leaving a lattice site, and the colour field due to particles at neighbouring lattice sites, respectively. The local colour flux is the difference between the two outgoing colour momenta at a site, while the colour field is defined to be the direction-weighted sum of the signed colour density at nearest neighbours. The Rothman-Keller collision rules were designed such that the "work" performed by the flux against the field is minimized, subject to the constraints of mass and momentum conservation. This effectively results in sending coloured particles towards regions of like colour, hence inducing cohesion and immiscible behaviour. Since then, lattice Boltzmann versions of this model have been introduced (Gunstensen *et. al.* 1991), and much research has been carried out on the theory (Rothman & Zaleski 1994), computer implementation (Gunstensen 1992), and phenomenology (Rothman & Zaleski 1994) of these models. In this section, we show that the Rothman-Keller model can be derived from an individual particle description, that will allow us to more easily motivate its generalisation to include surfactant particles.

We work on a D-dimensional lattice, $\mathcal{L}$, with n lattice vectors per site. We denote the lattice vectors by $\mathbf{c}_i$, where $i \in \{1, \dots, n\}$; we note that rest particles can be accommodated in this framework by a corresponding zero lattice vector. The state of the Rothman-Keller model for M immiscible species at time t is then completely specified by the quantities $n_i(\mathbf{x}, t) \in \{0, \dots, M\}$, where $i \in \{1, \dots, n\}$ and $\mathbf{x} \in \mathcal{L}$. We have $n_i(\mathbf{x}, t) = \alpha$ if there is a particle of colour $\alpha \in \{1, \dots, M\}$ with velocity $\mathbf{c}_i$ at position $\mathbf{x}$ at time t, and $n_i(\mathbf{x}, t) = 0$ otherwise. Thus, each site can be in any one of $(M+1)^n$ different states. We sometimes find it convenient to use the alternative representation,

$$n_i^\alpha(\mathbf{x}, t) \equiv \delta_{\alpha, n_i(\mathbf{x}, t)},$$

where $\delta_{\alpha, \beta}$ is the Kronecker delta, though we note that the $n_i^\alpha(\mathbf{x}, t) \in \{0, 1\}$ are not all independent since there can be at most one particle of any colour at a particular position, velocity, and time.

The evolution of the lattice gas for one generation takes place in two substeps. In the *propagation* substep, the particles simply move along their corresponding lattice vectors,

$$n_i(\mathbf{x} + \mathbf{c}_i, t + \Delta t) \leftarrow n_i(\mathbf{x}, t).$$

This is followed by the *collision* substep, in which the newly arrived particles change their state in a manner that conserves the mass of each species,

$$\rho^\alpha(\mathbf{x}, t) \equiv \sum_i^n n_i^\alpha(\mathbf{x}, t), \tag{1}$$

as well as the total D-dimensional momentum,

$$\mathbf{p}(\mathbf{x}, t) \equiv \sum_\alpha^M \sum_i^n \frac{\mathbf{c}_i}{\Delta t} n_i^\alpha(\mathbf{x}, t), \tag{2}$$

where we have assumed for simplicity that the particles carry unit mass.

To further specify the collision process, we partition the $(M+1)^n$ different states of a site into equivalence classes of states that have the same values for the $M + D$ conserved quantities (M conserved masses and D conserved components of momentum). Appendix A contains further information on the derivation of these equivalence classes. Collisions are thus required to take a state s to another state s' within the same equivalence class. If the equivalence class is of size one, as it would be if there were only one incoming particle, this uniquely specifies the collision process. For the more usual case in which there are many possible outgoing states, we must specify how to choose a single outcome.

We first consider the case of only two immiscible species ($M = 2$); we denote their colours by $\alpha = B$ or "blue" for water, and $\alpha = R$ or "red" for oil. In order to give these two phases cohesion, the Rothman-Keller model (Rothman & Keller 1988) favours collision outcomes that send particles of a given colour to neighbouring sites that are already dominated by that colour. To quantify this, we first define the *colour charge* of the particle moving in direction j at position $\mathbf{x}$ at time t,

$$q_j(\mathbf{x}, t) \equiv n_j^R(\mathbf{x}, t) - n_j^B(\mathbf{x}, t), \tag{3}$$

and the total colour charge at a site,

$$q(\mathbf{x}, t) \equiv \sum_j^n [n_j^R(\mathbf{x}, t) - n_j^B(\mathbf{x}, t)]$$
$$= \rho^R(\mathbf{x}, t) - \rho^B(\mathbf{x}, t).$$

We imagine that a colour charge q induces a *colour potential*, $\phi(r) = qf(r)$, at a distance r away from it, where $f(r)$ is some function defining the type and strength of the potential. Its energy of interaction with another colour charge q' is then $H_{cc} = q'\phi(r) = qq'f(r)$.

Since the collision part of the evolution process of the lattice gas conserves both the mass of each species and the total D-dimensional momentum, the only contribution to the interaction energy will come from the propagation phase, where the outgoing colour charges do work in moving to their new sites. Hence, we consider the interaction energy between the outgoing particle with colour charge $q_i'(\mathbf{x}, t)$ at $\mathbf{x} \in \mathcal{L}$, and the total colour charge $q(\mathbf{x} + \mathbf{y}, t)$ at site $\mathbf{x} + \mathbf{y} \in \mathcal{L}$. If we make an infinitesimal virtual displacement of the first charge from $\mathbf{x}$ to $\mathbf{x} + \delta\mathbf{x}$ (not necessarily on a lattice site), the corresponding change in interaction energy is

$$\delta H_{cc}(\mathbf{x}, t) = q_i'(\mathbf{x}, t)q(\mathbf{x} + \mathbf{y}, t)[f(|\mathbf{y} - \delta\mathbf{x}|) - f(|\mathbf{y}|)].$$

Taylor-expanding in $\delta\mathbf{x}$, this becomes

$$\delta H_{cc}(\mathbf{x}, t) = q_i'(\mathbf{x}, t)q(\mathbf{x} + \mathbf{y}, t)f_1(y)\mathbf{y} \cdot \delta\mathbf{x},$$

where $y = |\mathbf{y}|$, and where we have defined

$$f_\ell(y) \equiv \left(-\frac{1}{y}\frac{d}{dy}\right)^\ell f(y) \tag{4}$$

(ℓ being a positive integer or zero), giving a concise form for the derivatives of the function f(y). Since the outgoing particle with colour charge q' will move in the direction $\mathbf{c}_i$, we let $\delta\mathbf{x} \to \mathbf{c}_i$. We then sum over all outgoing colour charges i at site $\mathbf{x}$, and over all sites $\mathbf{y} \in \mathcal{L}$ with which they might interact to get the total *colour work*,

$$\Delta H_{cc}(\mathbf{x}, t) = \sum_i^n \sum_{\mathbf{y} \in \mathcal{L}} q_i'(\mathbf{x}, t)q(\mathbf{x} + \mathbf{y}, t)f_1(y)\mathbf{y} \cdot \mathbf{c}_i$$
$$= \left(\sum_i^n \frac{\mathbf{c}_i}{\Delta t}q_i'(\mathbf{x}, t)\right) \cdot \left(\sum_{\mathbf{y} \in \mathcal{L}} f_1(y)\mathbf{y}q(\mathbf{x} + \mathbf{y}, t)\right)\Delta t$$
$$= \mathbf{J}(\mathbf{x}, t) \cdot \mathbf{E}(\mathbf{x}, t)\Delta t,$$

where we have defined the *colour flux* of an outgoing state,

$$\mathbf{J}(\mathbf{x}, t) \equiv \sum_i^n \frac{\mathbf{c}_i}{\Delta t}q_i'(\mathbf{x}, t), \tag{5}$$

and the *colour field*,

$$\mathbf{E}(\mathbf{x}, t) \equiv \sum_{\mathbf{y} \in \mathcal{L}} f_1(y) \mathbf{y} q(\mathbf{x} + \mathbf{y}, t). \tag{6}$$

The sum over $\mathbf{y}$ extends over the range of the colour interaction, and will be discussed at length in Sec. IV E. The above expression for the colour work is identical to that used by Rothman and Keller if the *stencil function* $f_1(y)$ is chosen to select only nearest neighbour sites. The stencil function will be discussed in more detail in Section IV E. For now, we note that we were able to derive the Rothman-Keller model from the simple assumption that the particles interact with a potential function $\phi(r)$.

Note that we have intentionally used notation that highlights the analogy of the Rothman-Keller model to electrostatics. Specifically, the colour charge, potential, field and flux are analogous to the electrostatic charge, potential, field, and the current density, respectively. The colour work can then be imagined as a sort of "resistive heating" resulting from moving the current of outgoing colour charges against the colour field in one timestep.

The Rothman-Keller prescription is then to choose the outgoing state that minimizes ΔH_{cc}, since this is the one that most effectively sends particles up the gradient of colour and thereby induces cohesion. If multiple outgoing states yield the same minimal value of ΔH_{cc}, then the outcome is chosen randomly from among them. Rothman and Keller observed that this prescription yields phase separation when the total particle density on the lattice exceeds a critical value. Defining the reduced density of a lattice gas as the average proportion of underlying vectors at an individual lattice site that will contain a particle of some kind, Rothman and Keller found that the critical minimum value of reduced density needed for phase separation was approximately 0.2.

This prescription was subsequently generalized by Chan & Liang (1990) who noted that the colour work, ΔH_{cc}, can be thought of as a Hamiltonian function, $H(s, s')$, of the incoming and outgoing states; and they argued that this Hamiltonian should then be used to construct Boltzmann weights for choosing the outgoing state. Specifically, if $\mathcal{C}(s)$ denotes the equivalence class of states with the same conserved quantities as state s, then one can define a *partition function* for each equivalence class,

$$Z(s) = \sum_{s' \in \mathcal{C}(s)} e^{-\beta H(s, s')}, \tag{7}$$

where $1/\beta$ is a temperature-like parameter. We then define the collisional state-transition probabilities,

$$A(s \to s') = \begin{cases} \frac{1}{Z(s)} e^{-\beta H(s, s')} & \text{if } s' \in \mathcal{C}(s) \\ 0 & \text{otherwise} \end{cases}$$

These transition probabilities are normalized, so that

$$\sum_{s'} A(s \to s') = 1,$$

but they generally do not obey the condition of semi-detailed balance,

$$\sum_{s} A(s \to s') = 1,$$

except as $\beta \to 0$. Note that this reduces to the Rothman-Keller model as $\beta \to \infty$, and to the FHP model with no interactions as $\beta \to 0$. Indeed, Chan and Liang observed that the phase transition to immiscibility occurs for a critical value of β as well as of density. More generally, the Chan-Liang prescription is very useful for constructing lattice particle simulations that include an interaction Hamiltonian H in a manner consistent with the conservation of mass and momentum.

IV. A LATTICE GAS MODEL OF MICROEMULSIONS

To model microemulsions, we would like to introduce surfactant molecules in the framework of the Rothman-Keller lattice gas. To do this, we first introduce a third species index, say S, to represent the

presence or absence of a surfactant molecule. Thus, since $M = 3$, each site can be in any one of 4^n states, and can therefore be conveniently represented by $2n$ bits.

Surfactant molecules do not contribute to the colour flux and colour field in the same manner as ordinary coloured particles. Real surfactant molecules generally consist of a hydrophilic (often ionic) portion attached to a hydrophobic (hydrocarbon) portion. Thus, to pursue the electrostatic analogy mentioned in Sec. III, surfactant particles are best imagined as *colour dipoles*.

As in electrostatics, we shall model a colour dipole as a pair of equal and opposite colour charges, $\pm q$, separated by a fixed displacement, $\mathbf{a}$, in the limit as $\mathbf{a} \to 0$, $q \to \infty$, and $q\mathbf{a} \to \boldsymbol{\sigma}$ where $\boldsymbol{\sigma}$ is the colour dipole vector. Thus, we characterize the surfactant molecule at position $\mathbf{x}$ moving in direction i by a colour dipole vector $\boldsymbol{\sigma}_i(\mathbf{x}, t)$. Note that the value of $\boldsymbol{\sigma}_i(\mathbf{x}, t)$ is zero unless $n_i^S(\mathbf{x}, t) = 1$. The total dipolar vector at a site is then denoted by

$$\boldsymbol{\sigma}(\mathbf{x}, t) \equiv \sum_i^n \boldsymbol{\sigma}_i(\mathbf{x}, t). \tag{8}$$

It will be necessary to take scalar products of colour dipole vectors with other vector and tensor quantities. Beyond this, however, we leave their precise representation unspecified for the moment.

A. The Colour / Dipolar Field Interaction

We first consider the work done by a colour charge, Q, moving in the field of a fixed colour dipole, $\boldsymbol{\sigma}$, at a displacement $\mathbf{y}$, as shown in Fig. 1.
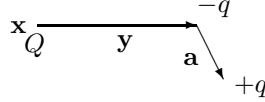

FIG. 1. *Model of Colour-Dipole Interaction*

The energy of the static interaction is

$$H_{\text{cd}} = qQ \left[+f(|\mathbf{y} + \mathbf{a}|) - f(|\mathbf{y}|) \right].$$

In the limit as $\mathbf{a} \to 0$ and $q \to \infty$, so that $q\mathbf{a} \to \boldsymbol{\sigma}$, this becomes

$$H_{\text{cd}} = -f_1(y)Q\boldsymbol{\sigma} \cdot \mathbf{y}.$$

Since the mass and momentum of particles with colour charge $q(\mathbf{x}, t)$ at $\mathbf{x} \in \mathcal{L}$ are the same before and after the collision part of the time evolution process, that is colour charge is conserved by the dynamics, the only local energy change that we need to incorporate into the Hamiltonian due to the above interaction comes about as a result of the outgoing particles doing work in moving to their new sites. To compute this energy change, we note that the interaction energy between an outgoing particle with colour charge $q_i'(\mathbf{x}, t)$ at $\mathbf{x} \in \mathcal{L}$ and the total dipolar vector $\boldsymbol{\sigma}(\mathbf{x} + \mathbf{y}, t)$ at site $\mathbf{x} + \mathbf{y} \in \mathcal{L}$ is given by

$$H_{\text{cd}} = -f_1(y)q_i'(\mathbf{x}, t)\boldsymbol{\sigma}(\mathbf{x} + \mathbf{y}, t) \cdot \mathbf{y}$$

and that if we make an infinitesimal virtual displacement of the particle from $\mathbf{x}$ to $\mathbf{x} + \delta\mathbf{x}$ (not necessarily on a lattice site), the corresponding change in the interaction energy, $H_{\text{cd}}(\mathbf{y} - \delta\mathbf{x}) - H_{\text{cd}}(\mathbf{y})$ is

$$\delta H_{\rm cd}(\mathbf{x},t) = -q_i'(\mathbf{x},t)\boldsymbol{\sigma}(\mathbf{x}+\mathbf{y},t) \cdot [f_2(y)\mathbf{y}\mathbf{y} - f_1(y)\mathbf{1}] \cdot \delta\mathbf{x},$$

where $f_\ell(y)$ is defined by Eq. (4). Since the outgoing particle with colour charge $q_i'(\mathbf{x},t)$ will move in direction $\mathbf{c}_i$, we let $\delta\mathbf{x} \to \mathbf{c}_i$. We then sum over all outgoing colour charges i at site $\mathbf{x}$, and over all sites $\mathbf{y} \in \mathcal{L}$ with which they might interact to get the total work, $\Delta H_{\rm cd}$. We find

$$\Delta H_{\rm cd}(\mathbf{x},t) = \mathbf{J}(\mathbf{x},t) \cdot \mathbf{P}(\mathbf{x},t)\Delta t,$$

where we have defined the *dipolar field* vector,

$$\mathbf{P}(\mathbf{x},t) \equiv -\sum_{\mathbf{y}\in\mathcal{L}} [f_2(y)\mathbf{y}\mathbf{y} - f_1(y)\mathbf{1}] \cdot \boldsymbol{\sigma}(\mathbf{x}+\mathbf{y},t), \tag{9}$$

and where $\mathbf{1}$ denotes the rank-two unit tensor.

Thus, we see that the effect of the dipoles at neighbouring sites is to augment the colour field felt by a colour charge by the amount $\mathbf{P}$. The total work done by the outgoing particles with colour charge is then

$$\Delta H_{\rm cc} + \Delta H_{\rm cd} = \mathbf{J} \cdot (\mathbf{E} + \mathbf{P})\,\Delta t.$$

We must now compute the work done by the outgoing dipoles.

B. The Dipole / Colour Field Interaction

Next, we consider the work done by a colour dipole vector, $\boldsymbol{\sigma}$, moving in the field of a fixed colour charge, Q, at a displacement $\mathbf{y}$ as shown in Fig. 2.
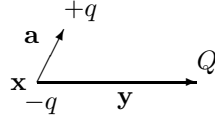

FIG. 2. *Model of Dipole-Colour Interaction*

The energy of the static interaction is

$$H_{\rm dc} = qQ\left[+f(|\mathbf{y} - \mathbf{a}|) - f(|\mathbf{y}|)\right].$$

In the limit as $\mathbf{a} \to 0$ and $q \to \infty$, so that $q\mathbf{a} \to \boldsymbol{\sigma}$, this becomes

$$H_{\rm dc} = +f_1(y)Q\boldsymbol{\sigma} \cdot \mathbf{y}.$$

In contrast to the case of the outgoing colour charge, the moments of the colour dipole vectors are not necessarily conserved by the collision phase of the update, and so the total local energy change which must be represented here has two parts to it. The first part, at *zeroth*-order, is due to the possibility of the postcollisional configuration having a different energy from the precollisional configuration, and the second, at *first*-order, is an energy change resulting from the outgoing colour dipoles doing work in moving to their new sites. Now, note that the interaction energy between an outgoing dipole with dipolar vector $\boldsymbol{\sigma}_i'(\mathbf{x},t)$ at $\mathbf{x} \in \mathcal{L}$, and the total colour charge, $q(\mathbf{x}+\mathbf{y},t)$, at site $\mathbf{x}+\mathbf{y} \in \mathcal{L}$ is given by

$$H_{\rm dc}(\mathbf{x},t) = +f_1(y)q(\mathbf{x}+\mathbf{y},t)\boldsymbol{\sigma}_i'(\mathbf{x},t) \cdot \mathbf{y}, \tag{10}$$

8

and that, if we make an infinitesimal virtual displacement of the dipole from $\mathbf{x}$ to $\mathbf{x} + \delta\mathbf{x}$ (not necessarily on a lattice site), the corresponding change in the interaction energy, $H_{\mathrm{dc}}(\mathbf{y} - \delta\mathbf{x}) - H_{\mathrm{dc}}(\mathbf{y})$, is

$$\delta H_{\mathrm{dc}}(\mathbf{x}, t) = q(\mathbf{x} + \mathbf{y}, t) \left[f_2(y)\boldsymbol{\sigma}_i'(\mathbf{x}, t) \cdot \mathbf{y}\mathbf{y} - f_1(y)\boldsymbol{\sigma}_i'(\mathbf{x}, t) \right] \cdot \delta\mathbf{x}, \tag{11}$$

where $f_\ell(y)$ is defined by Eq. (4). The zeroth order part of the total change in the interaction energy is then obtained directly from Eq. (10) and, letting $\delta\mathbf{x} \to \mathbf{c}_i$, we can get the first order part from Eq. (11). Hence the total change in the interaction energy, $\delta_T H_{\mathrm{dc}}$, is

$$\delta_T H_{\mathrm{dc}} = f_1(y)q(\mathbf{x} + \mathbf{y}, t)\boldsymbol{\sigma}_i'(\mathbf{x}, t) \cdot \mathbf{y} + q(\mathbf{x} + \mathbf{y}, t) \left[f_2(y)\boldsymbol{\sigma}_i'(\mathbf{x}, t) \cdot \mathbf{y}\mathbf{y} - f_1(y)\boldsymbol{\sigma}_i'(\mathbf{x}, t) \right] \cdot \mathbf{c}_i.$$

We then sum over all outgoing colour dipoles i at site $\mathbf{x}$, and over all sites $\mathbf{y} \in \mathcal{L}$ with which they might interact to get the total *dipolar color work*, ΔH_{dc}. We find, using Eq. (6),

$$\Delta H_{\mathrm{dc}}(\mathbf{x}, t) = \boldsymbol{\sigma}'(\mathbf{x}, t) \cdot \mathbf{E}(\mathbf{x}, t) + \mathcal{J}(\mathbf{x}, t) : \mathcal{E}(\mathbf{x}, t)\Delta t,$$

where the "double-dot" notation is short for $\mathrm{Tr}(\mathcal{J} \cdot \mathcal{E})$, and we have defined the *total outgoing dipole vector*

$$\boldsymbol{\sigma}'(\mathbf{x}, t) \equiv \sum_i^n \boldsymbol{\sigma}_i'(\mathbf{x}, t),$$

the *dipolar flux tensor*

$$\mathcal{J}(\mathbf{x}, t) \equiv \sum_i^n \frac{\mathbf{c}_i}{\Delta t}\boldsymbol{\sigma}_i'(\mathbf{x}, t), \tag{12}$$

and the *colour field gradient tensor*

$$\mathcal{E}(\mathbf{x}, t) \equiv \sum_{\mathbf{y} \in \mathcal{L}} q(\mathbf{x} + \mathbf{y}, t) \left[f_2(y)\mathbf{y}\mathbf{y} - f_1(y)\mathbf{1} \right], \tag{13}$$

and where $\mathbf{1}$ denotes the rank-two unit tensor.

Thus, just as the change in colour interaction energy ΔH_{cc} due to an outgoing configuration of colour charges was modelled by Rothman and Keller as the dot product of a vector flux and a vector field, we find that the analogous change ΔH_{dc} due to an outgoing configuration of colour *dipoles* can be modelled by the *double* dot product of a tensor flux and a tensor field, together with the addition of a zeroth order term which depends on the colour field vector itself. To complete the model we need to look at the interaction energy between two dipoles.

C. The Dipole / Dipole Interaction

We finally consider the work done by a colour dipole, $\boldsymbol{\sigma}_1$, moving in the field of a fixed colour dipole, $\boldsymbol{\sigma}_2$, at a displacement $\mathbf{y}$. To compute the static interaction energy between these two dipoles, we return to our fiducial model of a dipole as a pair of opposite charges, $\pm q$, separated by a fixed displacement, $\mathbf{a}$. Two such dipoles, separated by a distance vector $\mathbf{y}$, and distinguished by subscripts 1 and 2, are shown in Fig. 3.
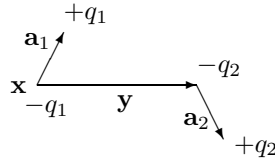

FIG. 3. *Model of Dipole-Dipole Interaction*

The static interaction energy between the dipoles is then

$$H_{\mathrm{dd}} = q_1 q_2 \left[-f(|\mathbf{y} - \mathbf{a}_1|) - f(|\mathbf{y} + \mathbf{a}_2|) + f(|\mathbf{y} + \mathbf{a}_2 - \mathbf{a}_1|) + f(|\mathbf{y}|) \right].$$

In the limit as $\mathbf{a}_j \to \infty$ and $q_j \to 0$, so that $q_j \mathbf{a}_j \to \boldsymbol{\sigma}_j$, this becomes

$$H_{\mathrm{dd}} = -f_2(y)(\boldsymbol{\sigma}_1 \cdot \mathbf{y})(\boldsymbol{\sigma}_2 \cdot \mathbf{y}) + f_1(y)\boldsymbol{\sigma}_1 \cdot \boldsymbol{\sigma}_2.$$

The analysis of the total interaction energy here is as in the dipole-colour field case above, since again we have the presence of both zeroth and first order terms to consider. Similarly, note that the interaction energy between an outgoing dipole with dipolar vector $\boldsymbol{\sigma}_i'(\mathbf{x}, t)$ at $\mathbf{x} \in \mathcal{L}$, and the total dipolar vector, $\boldsymbol{\sigma}(\mathbf{x} + \mathbf{y}, t)$, at site $\mathbf{x} + \mathbf{y} \in \mathcal{L}$ is given by

$$H_{\mathrm{dd}}(\mathbf{x}, t) = -f_2(y)(\boldsymbol{\sigma}_i'(\mathbf{x}, t) \cdot \mathbf{y})(\boldsymbol{\sigma}(\mathbf{x} + \mathbf{y}, t) \cdot \mathbf{y}) + f_1(y)\boldsymbol{\sigma}_i'(\mathbf{x}, t) \cdot \boldsymbol{\sigma}(\mathbf{x} + \mathbf{y}, t). \tag{14}$$

and that if we make an infinitesimal virtual displacement of the first dipole from $\mathbf{x}$ to $\mathbf{x} + \delta \mathbf{x}$ (not necessarily on a lattice site), the corresponding change in the interaction energy, $H_{\mathrm{dd}}(\mathbf{y} - \delta \mathbf{x}) - H_{\mathrm{dd}}(\mathbf{y})$, is

$$\begin{aligned} \delta H_{\mathrm{dd}}(\mathbf{x}, t) = f_2(y) & \left\{ [\boldsymbol{\sigma}_i'(\mathbf{x}, t) \cdot \boldsymbol{\sigma}(\mathbf{x} + \mathbf{y}, t)] \mathbf{y} + [\boldsymbol{\sigma}(\mathbf{x} + \mathbf{y}, t) \cdot \mathbf{y}] \boldsymbol{\sigma}_i'(\mathbf{x}, t) \right. \\ & \left. + [\boldsymbol{\sigma}_i'(\mathbf{x}, t) \cdot \mathbf{y}] \boldsymbol{\sigma}(\mathbf{x} + \mathbf{y}, t) \right\} \cdot \delta \mathbf{x} - f_3(y) [\boldsymbol{\sigma}(\mathbf{x} + \mathbf{y}, t) \cdot \mathbf{y}] [\boldsymbol{\sigma}_i'(\mathbf{x}, t) \cdot \mathbf{y}] \mathbf{y} \cdot \delta \mathbf{x}, \end{aligned} \tag{15}$$

where the $f_\ell(y)$ are given by Eq. (4). Consequently we can use Eq. (14) to obtain the zeroth order energy change, while, since the outgoing dipole with dipolar vector $\boldsymbol{\sigma}_i'(\mathbf{x}, t)$ will move in direction $\mathbf{c}_i$, letting $\delta \mathbf{x} \to \mathbf{c}_i$ enables us to obtain the first order part directly from Eq. (15). The total change in the interaction energy, $\delta_T H_{\mathrm{dd}}$, is then given by

$$\begin{aligned} \delta_T H_{\mathrm{dd}} = & -f_2(y)(\boldsymbol{\sigma}_i'(\mathbf{x}, t) \cdot \mathbf{y})(\boldsymbol{\sigma}(\mathbf{x} + \mathbf{y}, t) \cdot \mathbf{y}) + f_1(y)\boldsymbol{\sigma}_i'(\mathbf{x}, t) \cdot \boldsymbol{\sigma}(\mathbf{x} + \mathbf{y}, t) \\ & + f_2(y) \left\{ [\boldsymbol{\sigma}_i'(\mathbf{x}, t) \cdot \boldsymbol{\sigma}(\mathbf{x} + \mathbf{y}, t)] \mathbf{y} + [\boldsymbol{\sigma}(\mathbf{x} + \mathbf{y}, t) \cdot \mathbf{y}] \boldsymbol{\sigma}_i'(\mathbf{x}, t) \right. \\ & \left. + [\boldsymbol{\sigma}_i'(\mathbf{x}, t) \cdot \mathbf{y}] \boldsymbol{\sigma}(\mathbf{x} + \mathbf{y}, t) \right\} \cdot \delta \mathbf{x} - f_3(y) [\boldsymbol{\sigma}(\mathbf{x} + \mathbf{y}, t) \cdot \mathbf{y}] [\boldsymbol{\sigma}_i'(\mathbf{x}, t) \cdot \mathbf{y}] \mathbf{y} \cdot \delta \mathbf{x}. \end{aligned}$$

We then sum over all outgoing colour dipoles i at site $\mathbf{x}$, and over all sites $\mathbf{y} \in \mathcal{L}$ with which they might interact to get the total *interdipolar colour work*, ΔH_{dd}. After some manipulation, and making use of Eq. (9), we find that the result is

$$\Delta H_{\mathrm{dd}}(\mathbf{x}, t) = \boldsymbol{\sigma}'(\mathbf{x}, t) \cdot \mathbf{P}(\mathbf{x}, t) + \mathcal{J}(\mathbf{x}, t) : \mathcal{P}(\mathbf{x}, t)\Delta t,$$

where $\mathcal{J}(\mathbf{x}, t)$ is the dipolar flux tensor, and we have defined the *dipolar field gradient* tensor

$$\mathcal{P}(\mathbf{x}, t) = -\sum_{\mathbf{y} \in \mathcal{L}} \boldsymbol{\sigma}(\mathbf{x} + \mathbf{y}, t) \cdot [f_3(y)\mathbf{y}\mathbf{y}\mathbf{y} - f_2(y)\mathbf{y} \cdot \boldsymbol{\Omega}], \tag{16}$$

wherein we have in turn defined the completely symmetric and isotropic fourth-rank tensor,

$$\Omega_{ijkl} \equiv \delta_{ij}\delta_{kl} + \delta_{ik}\delta_{jl} + \delta_{il}\delta_{jk}.$$

D. Expression for the Total Colour Work

The total interaction work can now be written

$$\begin{aligned} \Delta H_{\mathrm{int}} &= \Delta H_{\mathrm{cc}} + \Delta H_{\mathrm{cd}} + \Delta H_{\mathrm{dc}} + \Delta H_{\mathrm{dd}} \\ &= \left[\left(\mathbf{J} + \frac{\boldsymbol{\sigma}'}{\Delta t} \right) \cdot (\mathbf{E} + \mathbf{P}) + \mathcal{J} : (\mathcal{E} + \mathcal{P}) \right] \Delta t. \end{aligned}$$

The work done to change the kinetic energy is then

$$\Delta H_{\text{ke}} = \sum_{\alpha}^{M} \sum_{i}^{n} \frac{|\mathbf{c}_i|^2}{2} \left[n_i^{\alpha\prime}(\mathbf{x}, t) - n_i^{\alpha}(\mathbf{x}, t) \right]. \tag{17}$$

The total work done is then

$$\Delta H_{\text{total}} = \Delta H_{\text{int}} + \Delta H_{\text{ke}}. \tag{18}$$

We note that the change in kinetic energy was not included by Rothman and Keller in their model; neither has it been used in subsequent studies of their model. On the other hand, we can think of no good reason to omit it. Its presence or absence will not affect the equilibrium properties of the model, but may impact its nonequilibrium properties.

E. Stencils

We would like to use the total work, ΔH_{total} as the Hamiltonian in an implementation of the Chan-Liang procedure. To compute this, we will first need the *colour flux* and the *dipolar flux* tensor. These are easily computed directly from their definitions, Eqs. (5) and (12) respectively. Their computation involves only quantities that are local to the site $\mathbf{x}$.

We will also need the *colour field*, the *colour field gradient* tensor, and the *dipolar field gradient* tensor. These are given by Eqs. (6), (13), and (16), respectively. Note that these expressions involve various derivatives of the potential function $f(y)$, as defined in Eq. (4). In order to develop a tractable lattice model, however, we shall want to truncate the range of this function, and so it is unclear how we should treat its derivatives. In this section, we shall show how to define a single function, $g(\mathbf{y})$, which parametrizes the interparticle potential, and in terms of which we can derive the fields by taking linear combinations of quantities from some pattern of neighbouring sites. These combinations, called *stencils*, involve $g(\mathbf{y})$ but do *not* involve its derivatives at all. We are then free to truncate $g(\mathbf{y})$ in order to develop a model that involves only nearest neighbour communication on the grid.

A stencil can be specified as follows: suppose that we have a scalar field $A(\mathbf{x})$. Let each site $\mathbf{x}$ retrieve the value $A(\mathbf{x} + \mathbf{y})$ from its neighbour at displacement $\mathbf{y}$, multiply it by the coefficient $g(\mathbf{y})$, and sum over all neighbours $\mathbf{y}$. The result,

$$\sum_{\mathbf{y} \in \mathcal{L}} g(\mathbf{y}) A(\mathbf{x} + \mathbf{y}),$$

is called the *scalar stencil* of the scalar field A. We can also define the *vector stencil*,

$$\sum_{\mathbf{y} \in \mathcal{L}} g(\mathbf{y}) \mathbf{y} A(\mathbf{x} + \mathbf{y}),$$

and the *tensor stencil*,

$$\sum_{\mathbf{y} \in \mathcal{L}} g(\mathbf{y}) \mathbf{y}\mathbf{y} A(\mathbf{x} + \mathbf{y}),$$

and so on. Likewise, given a vector field $\mathbf{B}(\mathbf{x})$ we can define its scalar stencil,

$$\sum_{\mathbf{y} \in \mathcal{L}} g(\mathbf{y}) \mathbf{B}(\mathbf{x} + \mathbf{y}),$$

vector stencil,

$$\sum_{\mathbf{y}\in\mathcal{L}} g(\mathbf{y})\mathbf{y}\mathbf{B}(\mathbf{x}+\mathbf{y}),$$

and so on. We require the following isotropy properties of the coefficients $g(\mathbf{y})$:

$$\sum_{\mathbf{y}\in\mathcal{L}} g(\mathbf{y}) = G_0$$

$$\sum_{\mathbf{y}\in\mathcal{L}} g(\mathbf{y})\,\mathbf{y} = 0$$

$$\sum_{\mathbf{y}\in\mathcal{L}} g(\mathbf{y})\,\mathbf{y}\mathbf{y} = G_2\mathbf{1}$$

$$\sum_{\mathbf{y}\in\mathcal{L}} g(\mathbf{y})\,\mathbf{y}\mathbf{y}\mathbf{y} = 0$$

$$\sum_{\mathbf{y}\in\mathcal{L}} g(\mathbf{y})\,\mathbf{y}\mathbf{y}\mathbf{y}\mathbf{y} = G_4\boldsymbol{\Omega}. \tag{19}$$

As a concrete example, consider a regular Bravais lattice ($|\mathbf{c}_i| = c$), such that all tensors up to the fourth order formed by the lattice vectors are isotropic,

$$\sum_j^n 1 = n$$

$$\sum_j^n \mathbf{c}_i = 0$$

$$\sum_j^n \mathbf{c}_i\mathbf{c}_i = \frac{n}{D}\mathbf{1}$$

$$\sum_j^n \mathbf{c}_i\mathbf{c}_i\mathbf{c}_i = 0$$

$$\sum_j^n \mathbf{c}_i\mathbf{c}_i\mathbf{c}_i\mathbf{c}_i = \frac{n}{D(D+2)}\boldsymbol{\Omega}. \tag{20}$$

By choosing the stencil coefficients

$$g(\mathbf{y}) = \begin{cases} 1 & \text{if } |\mathbf{y}| = c \\ 0 & \text{otherwise,} \end{cases} \tag{21}$$

we see at once that we have $G_0 = n$, $G_2 = n/D$, and $G_4 = n/[D(D+2)]$.

We note that lattice gases for fluid applications *must* have a lattice for which Eqs. (20) are satisfied in order to ensure isotropy of the resulting hydrodynamics, so it is always possible to use Eq. (21) to define a stencil for such a lattice gas. It is possible, however, by judicious choice of the coefficients $g(\mathbf{y})$ to satisfy isotropy conditions like Eqs. (19) to higher rank than those of the lattice vectors, Eqs. (20).

F. Stencils for the Colour Field and its Gradient

We first note that the colour field can be computed directly from its definition, Eq. (6), in a straightforward manner. It is a vector stencil of the colour charge, with stencil coefficients $f_1(y)$. We could likewise compute the colour field gradient tensor directly from its definition, Eq. (13), but there is a better way. Consider the colour field evaluated at a point $\mathbf{x}+\delta\mathbf{x}$ (not necessarily at a lattice site). We have

$$\mathbf{E}(\mathbf{x} + \delta\mathbf{x}, t) = \sum_{\mathbf{y} \in \mathcal{L}} f_1(|\mathbf{y} - \delta\mathbf{x}|)(\mathbf{y} - \delta\mathbf{x})q(\mathbf{x} + \mathbf{y}, t).$$

Expanding in $\delta\mathbf{x}$, this becomes

$$\mathbf{E}(\mathbf{x} + \delta\mathbf{x}, t) = \mathbf{E}(\mathbf{x}, t) + \left\{ \sum_{\mathbf{y} \in \mathcal{L}} q(\mathbf{x} + \mathbf{y}, t) \left[f_2(y)\mathbf{y}\mathbf{y} - f_1(y)\mathbf{1} \right] \right\} \cdot \delta\mathbf{x}$$
$$+ \left\{ \frac{1}{2} \sum_{\mathbf{y} \in \mathcal{L}} q(\mathbf{x} + \mathbf{y}, t) \left[f_3(y)\mathbf{y}\mathbf{y}\mathbf{y} - f_2(y)\mathbf{y} \cdot \boldsymbol{\Omega} \right] \right\} : \delta\mathbf{x}\delta\mathbf{x}.$$

If we now substitute $\delta\mathbf{x} \to \mathbf{z}$ in this equation, and use it to take the vector stencil of the field, we get

$$\sum_{\mathbf{z} \in \mathcal{L}} g(\mathbf{z})\mathbf{z}\mathbf{E}(\mathbf{x} + \mathbf{z}, t) = G_2 \sum_{\mathbf{y} \in \mathcal{L}} q(\mathbf{x} + \mathbf{y}) \left[f_2(y)\mathbf{y}\mathbf{y} - f_1(y)\mathbf{1} \right],$$

where we used Eqs. (19). Comparing this with Eq. (13), we see that the colour field gradient tensor is given by the vector stencil of the colour field,

$$\mathcal{E}(\mathbf{x}, t) = \frac{1}{G_2} \sum_{\mathbf{z} \in \mathcal{L}} g(\mathbf{z})\mathbf{z}\mathbf{E}(\mathbf{x} + \mathbf{z}, t). \tag{22}$$

In addition to justifying the name of this tensor, this equation is a much more efficient way to compute it in practice.

G. Stencils for the Dipolar Field and Dipolar Gradient

Finally, we need to compute the dipolar field and the dipolar field gradient tensor. Once again we could compute these directly from their definitions, Eqs. (9) and (16) respectively, but there is an easier way. We first define the scalar field,

$$S(\mathbf{x}, t) \equiv \sum_{\mathbf{y} \in \mathcal{L}} f_1(y)\mathbf{y} \cdot \boldsymbol{\sigma}(\mathbf{x} + \mathbf{y}, t), \tag{23}$$

using the same stencil coefficients $f_1(y)$ that we used to get the colour field. We then consider the value of this field at a point $\mathbf{x} + \delta\mathbf{x}$ (not necessarily at a lattice site). We have

$$S(\mathbf{x} + \delta\mathbf{x}, t) = \sum_{\mathbf{y} \in \mathcal{L}} f_1(|\mathbf{y} - \delta\mathbf{x}|)(\mathbf{y} - \delta\mathbf{x}) \cdot \boldsymbol{\sigma}(\mathbf{x} + \mathbf{y}, t).$$

Expanding in $\delta\mathbf{x}$, this becomes

$$S(\mathbf{x} + \delta\mathbf{x}, t) = S(\mathbf{x}, t) + \left\{ \sum_{\mathbf{y} \in \mathcal{L}} \boldsymbol{\sigma}(\mathbf{x} + \mathbf{y}, t) \cdot \left[f_2(y)\mathbf{y}\mathbf{y} - f_1(y)\mathbf{1} \right] \right\} \cdot \delta\mathbf{x}$$
$$+ \left\{ \frac{1}{2} \sum_{\mathbf{y} \in \mathcal{L}} \boldsymbol{\sigma}(\mathbf{x} + \mathbf{y}, t) \cdot \left[f_3(y)\mathbf{y}\mathbf{y}\mathbf{y} - f_2(y)\mathbf{y} \cdot \boldsymbol{\Omega} \right] \right\} : \delta\mathbf{x}\delta\mathbf{x}.$$

If we now substitute $\delta\mathbf{x} \to \mathbf{z}$ in this equation, and use it to take the scalar, vector, and tensor stencils of the scalar field $S(\mathbf{x}, t)$, we get

13

$$\sum_{\mathbf{z}\in\mathcal{L}} g(\mathbf{z})S(\mathbf{x}+\mathbf{z},t) = G_0 S(\mathbf{x},t) + \frac{G_2}{2}\sum_{\mathbf{y}\in\mathcal{L}}\boldsymbol{\sigma}(\mathbf{x}+\mathbf{y},t)\cdot\mathbf{y}\left[f_3(y)y^2 - (D+2)f_2(y)\right],$$

$$\sum_{\mathbf{z}\in\mathcal{L}} g(\mathbf{z})\mathbf{z}S(\mathbf{x}+\mathbf{z},t) = G_2\sum_{\mathbf{y}\in\mathcal{L}}\boldsymbol{\sigma}(\mathbf{x}+\mathbf{y},t)\cdot\left[f_2(y)\mathbf{y}\mathbf{y} - f_1(y)\mathbf{1}\right],$$

and

$$\sum_{\mathbf{z}\in\mathcal{L}} g(\mathbf{z})\mathbf{z}\mathbf{z}S(\mathbf{x}+\mathbf{z},t) = G_2 S(\mathbf{x},t)\mathbf{1} + \frac{G_4}{2}\mathbf{1}\sum_{\mathbf{y}\in\mathcal{L}}\boldsymbol{\sigma}(\mathbf{x}+\mathbf{y},t)\cdot\mathbf{y}\left[f_3(y)y^2 - (D+2)f_2(y)\right]$$

$$+ G_4\sum_{\mathbf{y}\in\mathcal{L}}\boldsymbol{\sigma}(\mathbf{x}+\mathbf{y},t)\cdot\left[f_3(y)\mathbf{y}\mathbf{y}\mathbf{y} - f_2(y)\mathbf{y}\cdot\boldsymbol{\Omega}\right]$$

respectively, where we used Eqs. (19). Comparing these with Eqs. (9) and (16), we see that we can write

$$\mathbf{P}(\mathbf{x},t) = -\frac{1}{G_2}\sum_{\mathbf{z}\in\mathcal{L}} g(\mathbf{z})\mathbf{z}S(\mathbf{x}+\mathbf{z},t), \tag{24}$$

and

$$\mathcal{P}(\mathbf{x},t) = \left(\frac{G_2}{G_4} - \frac{G_0}{G_2}\right)\mathbf{1}S(\mathbf{x},t) - \sum_{\mathbf{z}\in\mathcal{L}} g(\mathbf{z})\left(\frac{\mathbf{z}\mathbf{z}}{G_4} - \frac{\mathbf{1}}{G_2}\right)S(\mathbf{x}+\mathbf{z},t), \tag{25}$$

which are efficient methods to compute the dipolar field vector and the dipolar field gradient tensor, respectively.

H. Sampling the Outgoing State

We have not yet specified the exact representation of the colour dipole vectors. As has been noted, it is necessary that there be a colour dipole vector $\boldsymbol{\sigma}_i(\mathbf{x},t)$ associated with each particle i at each site $\mathbf{x}$ at each time t, and that it be possible to take inner and outer products of this vector with other tensor quantities. We now further demand that the *magnitude* of each of these dipolar vectors be a fixed constant σ when there is a surfactant particle present, and be zero when there is not. That is, we have

$$\boldsymbol{\sigma}_i(\mathbf{x},t) = \sigma n_i^S(\mathbf{x},t)\hat{\boldsymbol{\sigma}}_i(\mathbf{x},t), \tag{26}$$

where the dipolar strength σ is an input parameter, and where $\hat{\boldsymbol{\sigma}}_i(\mathbf{x},t)$ is a unit vector in the direction of the dipolar orientation. This latter quantity can be parametrized by $D-1$ real-valued angles for each direction $i = 1,\ldots,n$, for a total of $n(D-1)$ angles.

We use the Chan-Liang procedure with the Hamiltonian given by the total work, Eq. (18). In this Hamiltonian, we note that the fields depend only upon the incoming states, s, while the kinetic energy and the fluxes depend upon the outgoing state, s'. More specifically, the kinetic energy and the colour flux depend only upon the outgoing occupation numbers, $n_i^{\alpha\prime}(\mathbf{x},t)$, while the dipolar flux depends as well upon the outgoing dipolar orientations, $\hat{\boldsymbol{\sigma}}_i'(\mathbf{x},t)$.

With this in mind, we adopt the notation $s = (\mathbf{n},\hat{\boldsymbol{\sigma}})$, where $\mathbf{n}$ and $\hat{\boldsymbol{\sigma}}$ denote the occupation numbers and dipolar orientations of state s, respectively; likewise $s' = (\mathbf{n}',\hat{\boldsymbol{\sigma}}')$ denotes the outgoing state. We can then write the Hamiltonian in the following form:

$$H(s,s') = H_0(s,\mathbf{n}') + \left[\frac{\boldsymbol{\sigma}'}{\Delta t}\cdot[\mathbf{E}(\mathbf{n}) + \mathbf{P}(s)] + \mathcal{J}(s') : [\mathcal{E}(\mathbf{n}) + \mathcal{P}(s)]\right]\Delta t,$$

where

$$H_0(s, \mathbf{n}') \equiv \Delta H_{\text{ke}}(\mathbf{n}, \mathbf{n}') + \mathbf{J}(\mathbf{n}') \cdot [\mathbf{E}(\mathbf{n}) + \mathbf{P}(s)] \, \Delta t, \tag{27}$$

and where we have suppressed space and time dependences in favour of state dependences for clarity. Using Eqs. (12) and (26), we can then write

$$\left[\frac{\boldsymbol{\sigma}'}{\Delta t} \cdot [\mathbf{E}(\mathbf{n}) + \mathbf{P}(s)] + \mathcal{J}(s') : [\mathcal{E}(\mathbf{n}) + \mathcal{P}(s)] \right] \Delta t = \sum_i^n n_i^{S'} \hat{\boldsymbol{\sigma}}_i' \cdot \mathbf{A}_i(s),$$

where we have defined the vectors

$$\mathbf{A}_i(s) \equiv \sigma \left[(\mathbf{E}(\mathbf{n}) + \mathbf{P}(s)) + (\mathcal{E}(\mathbf{n}) + \mathcal{P}(s)) \cdot \mathbf{c}_i \Delta t \right] \tag{28}$$

for $i = 1, \ldots, n$.

The partition function of Eq. (7) is then obtained by summing over all possible outgoing occupation numbers and integrating over all outgoing dipolar orientations,

$$Z(s) = \sum_{\mathbf{n}'} e^{-\beta H_0(s, \mathbf{n}')} \int d\hat{\boldsymbol{\sigma}}_1' \cdots \int d\hat{\boldsymbol{\sigma}}_n' \exp \left[-\beta \sum_i^n n_i^{S'} \hat{\boldsymbol{\sigma}}_i' \cdot \mathbf{A}_i(s) \right]$$

$$= \sum_{\mathbf{n}'} e^{-\beta H_0(s, \mathbf{n}')} \prod_i^n \int d\hat{\boldsymbol{\sigma}}_i' \exp \left[-\beta n_i^{S'} \hat{\boldsymbol{\sigma}}_i' \cdot \mathbf{A}_i(s) \right].$$

The probability distribution of outgoing states is then

$$\mathcal{P}(\mathbf{n}', \hat{\boldsymbol{\sigma}}') = \frac{1}{Z(s)} e^{-\beta H(s, s')}.$$

The reduced probability distribution of outgoing occupation numbers (without regard to dipolar orientation) is then

$$P(\mathbf{n}') = \frac{1}{Z(s)} e^{-\beta H_0(s, \mathbf{n}')} \prod_i^n \int d\hat{\boldsymbol{\sigma}}_i' \exp \left[-\beta n_i^{S'} \hat{\boldsymbol{\sigma}}_i' \cdot \mathbf{A}_i(s) \right].$$

Our strategy shall be to first sample from $P(\mathbf{n}')$ to get the outgoing occupation numbers, $\mathbf{n}'$, and to then sample the dipolar orientations from

$$Q_i(\hat{\boldsymbol{\sigma}}_i') = \frac{\exp \left[-\beta n_i^{S'} \hat{\boldsymbol{\sigma}}_i' \cdot \mathbf{A}_i(s) \right]}{\int d\hat{\boldsymbol{\sigma}}_i' \exp \left[-\beta n_i^{S'} \hat{\boldsymbol{\sigma}}_i' \cdot \mathbf{A}_i(s) \right]}$$

for $i = 1, \ldots, n$.

For example, in two dimensions we can parametrize the orientations $\hat{\boldsymbol{\sigma}}_i'$ by the angles θ_i', so

$$\hat{\boldsymbol{\sigma}}_i' = \hat{\mathbf{x}} \cos \theta_i' + \hat{\mathbf{y}} \sin \theta_i'.$$

Writing $\mathbf{A}_i$ in polar form,

$$\mathbf{A}_i(s) = A_i(s) \left[\hat{\mathbf{x}} \cos \phi_i(s) + \hat{\mathbf{y}} \sin \phi_i(s) \right],$$

where

$$A_i(s) \equiv \sigma \left| [\mathcal{E}(\mathbf{n}) + \mathcal{P}(s)] \cdot \mathbf{c}_i + \mathbf{E}(\mathbf{n}) + \mathbf{P}(s) \right| \Delta t \tag{29}$$

and

$$\phi_i(s) \equiv \arg \left\{ (\hat{\mathbf{x}} + i\hat{\mathbf{y}}) \cdot ([\mathcal{E}(\mathbf{n}) + \mathcal{P}(s)] \cdot \mathbf{c}_i + \mathbf{E}(\mathbf{n}) + \mathbf{P}(s)) \right\}, \tag{30}$$

15

and performing the integration we see that the partition function is

$$Z(s) = (2\pi)^n \sum_{\mathbf{n}'} e^{-\beta H_0(s,\mathbf{n}')} \prod_i^n I_0(\beta n_i^{S'} A_i(s)),$$

where $I_0(z)$ is the modified Bessel function. The reduced probability distribution is then

$$P(\mathbf{n}') = \frac{(2\pi)^n}{Z(s)} e^{-\beta H_0(s,\mathbf{n}')} \prod_i^n I_0(\beta n_i^{S'} A_i(s)). \tag{31}$$

We sample the outgoing occupation numbers $\mathbf{n}'$ from this, and then determine the outgoing dipolar angles by sampling from

$$Q_i(\theta_i') = \frac{\exp\left[-\beta n_i^{S'} A_i(s) \cos(\theta_i' - \phi_i(s))\right]}{2\pi I_0(\beta n_i^{S'} A_i(s))} \tag{32}$$

for each i from 1 to n separately. Details of these sampling procedures are given in Appendix B. Note that in the absence of surfactant particles $\mathbf{n}' = 0$, so the Bessel functions are then all unity, and the model reduces to Chan and Liang's generalisation of the Rothman-Keller model (with the addition of the kinetic energy).

I. Summary of the Algorithm

We can now write down the full algorithm for our microemulsion lattice gas model. Consider, for example, a triangular grid in two dimensions ($D = 2$) with up to seven particles per site ($n = 7$) corresponding to the six lattice directions plus a rest particle. We use Eq. (21) for $g(\mathbf{y})$, from which it follows that $G_0 = 7$, $G_2 = 3$, and $G_4 = 3/4$. (Note that the rest particle does not contribute to G_2 and G_4.) The algorithm is then:

1. For all sites $\mathbf{x}$ and lattice vectors i, propagate particle $n_i(\mathbf{x}, t)$ and its respective dipolar angle $\theta_i(\mathbf{x}, t)$ to site $\mathbf{x} + \mathbf{c}_i$.

2. Each site $\mathbf{x}$ computes its colour charge $q(\mathbf{x}, t)$ according to Eq. (3).

3. Each site retrieves its neighbours' colour charges, and computes its colour field $\mathbf{E}(\mathbf{x}, t)$ using Eq. (6).

4. Each site retrieves its neighbours' colour fields, and computes its colour field gradient tensor $\mathcal{E}(\mathbf{x}, t)$ using Eq. (22).

5. Each site $\mathbf{x}$ computes its total dipole vector $\boldsymbol{\sigma}(\mathbf{x}, t)$ according to Eq. (8).

6. Each site retrieves its neighbours' total dipole vectors, and computes the scalar field $S(\mathbf{x}, t)$ according to Eq. (23).

7. Each site retrieves its neighbours' scalar fields S, and computes its dipolar field vector $\mathbf{D}(\mathbf{x}, t)$ and dipolar field gradient $\mathcal{D}(\mathbf{x}, t)$ according to Eqs. (24) and (25), respectively.

8. Each site computes its vectors $\mathbf{A}_i$ according to Eq. (28), and converts them to polar form according to Eqs. (29) and (30).

9. Each site uses its state s to determine its equivalance class $\mathcal{C}(s)$, and enumerate the allowed outgoing states s'.

10. For each outgoing state s', we compute the colour flux $\mathbf{J}(s')$ according to Eq. (5).

11. For each outgoing state s', we compute the kinetic energy change ΔH_{ke} according to Eq. (17).

12. For each outgoing state s', we compute the dipole-independent part of the Hamiltonian, $H_0(s, \mathbf{n}')$, according to Eq. (27).

13. For each outgoing configuration $\mathbf{n}'$, we calculate the probability $P(\mathbf{n}')$ according to Eq. (31), and normalize these over all outgoing configurations.

14. The final outgoing state $\mathbf{n}'$ is then sampled from $P(\mathbf{n}')$.

15. Given $\mathbf{n}'$, the final outgoing dipolar angles $\theta_i'(\mathbf{x}, t)$ are sequentially sampled from $Q_i(\theta_i')$ given by Eq. (32).

16. Go to step 1.

For simulations using our model on moderately sized lattices in $2D$ we have employed the algorithm as it is written above. For larger system sizes, however, it is possible that this algorithm may be prohibitive in terms of computer memory. In this case simpler versions may be worked out in which the dipolar vector directions are discrete rather than continuous, and/or in which a Metropolis Monte Carlo procedure is used to select the outgoing state. Although the simulations reported in this paper have been undertaken using a basic C code, the algorithm is parallelizable, using either the message-passing or data-parallel paradigms. We expect to use massively parallel supercomputers to achieve larger system sizes and later times in future simulations.

V. SIMULATIONS

As mentioned earlier there are certain basic properties of self-assembling amphiphilic systems that it is essential our model be able to reproduce. In this section, we describe some of these features and our efforts to reproduce them with the lattice-gas model defined above.

A. Common Properties of Microemulsions

In general, the addition of a small amount of surfactant to a system of oil and water will not alter the two-phase coexistence; the added amphiphile will partition itself between the two phases. However, if there is enough amphiphile present in the system to overcome the tendency of oil and water to phase separate, then a fluid phase can form in which the oil and water are solubilized and the surfactant tends to be ordered in some way. This can result in a finite concentration of oil-in-water (o/w) or water-in-oil (w/o) droplets, usually called *micelles*, forming within the fluid, or alternatively in the formation of sheets of amphiphile separating coherent regions of oil and water (sometimes called *lamellar phase*). If the concentrations of the oil and water in the system are not very different then both coherent regions will span the system, and the fluid is said to be *bicontinuous*. Fluids existing in these droplet and bicontinuous phases are termed microemulsions. Note that they are characterized by extensive amounts of internal interface.

Self-assembly also occurs in the two-component binary systems of water and amphiphile. The terms micelle and lamellae are also used in the binary case, when they refer to an often spherical cluster of surfactant molecules sitting within bulk water (or an inverse micelle if in bulk oil), and sheets of water separated by amphiphilic bilayers, respectively. Typically, at amphiphile concentrations below a critical value, called the *critical micelle concentration*, the amphiphile molecules exist as isolated *monomers* in the bulk water (or oil). Above the critical micelle concentration, the amphiphile molecules cluster into micelles of a characteristic average size, consisting of a well-defined number of monomers; although there are clusters of varying sizes present, the distribution of sizes is sharply peaked about one value. Lamellar phases are found at still higher amphiphile concentrations.

B. Definition of Coupling Constants

In order to incorporate the most general form of interaction energy within our model system, we introduce a set of coupling constants $\alpha, \mu, \epsilon, \zeta$, in terms of which the total interaction work can then be written as

$$\Delta H_{\text{int}} = \alpha \Delta H_{\text{cc}} + \mu \Delta H_{\text{cd}} + \epsilon \Delta H_{\text{dc}} + \zeta \Delta H_{\text{dd}}. \tag{33}$$

We carry out simulations using the algorithm described in Section $IV\,I$; however, we have not yet defined the functions $f_\ell(y)$ that appear in Eq. (4) - in particular we need to specify the value of $f_1(y)$ since it appears in all four of the terms in ΔH_{int}. Refering back to Eq. (6) we see that if we set

$$f_1(y) = \begin{cases} 1 & \text{if } y = 1 \\ 0 & \text{otherwise} \end{cases} \tag{34}$$

then we retrieve exactly the equation used by Rothman and Keller for their definition of the colour field. In the present paper, we shall employ this simple prescription and leave any more involved usage of stencils to a later date. Note that we also have to specify the temperature-like parameter β^{-1} (Eq. (7)), the kinetic energy term ΔH_{ke} (Eq. (17)), and the dipolar strength σ (Eq. (26)). Again, as simplifications for the current preliminary analysis of the model, we have set β and σ to unity and the kinetic energy change ΔH_{ke} to zero throughout. Unless otherwise stated, all results described below have been obtained using $2D$ lattices of grid size 128×128 with periodic boundary conditions in both dimensions. The colour pictures showing the time evolution of systems are coded as follows; black is equivalent to water, green to surfactant and red to oil.

C. Oil-Water System

We begin by noting that when no surfactant particles are present our model reduces to Chan and Liang's generalization of the Rothman-Keller model for two immiscible fluids (Rothman & Keller 1988). With no surfactant particles present in the system, the only term that contributes numerically to the collision process is $\alpha \Delta H_{\text{cc}}$. We set $\alpha = \beta = 1.0$ and perform a simulation that has a random initial configuration with equal amounts of oil and water in the system. The reduced density (i.e. the proportion of lattice vectors at each site that contain a particle) is 0.55. In this parameter regime, the Chan-Liang model does exhibit phase separation with positive surface tension, as is evident from Fig. 4, which illustrates the nonequilibrium behaviour of the immiscible lattice gas. In displaying the results graphically, we have used a majority rule to define the displayed colour of each site; if the numbers of oil and water particles at a site are equal then the displayed colour is selected randomly with probability $\frac{1}{2}$. The behaviour shown in the figure is, indeed, effectively the same as that obtained by Rothman and Keller. If left to run for a large enough time the system would eventually reach the completely separated state of two distinct layers of fluid.
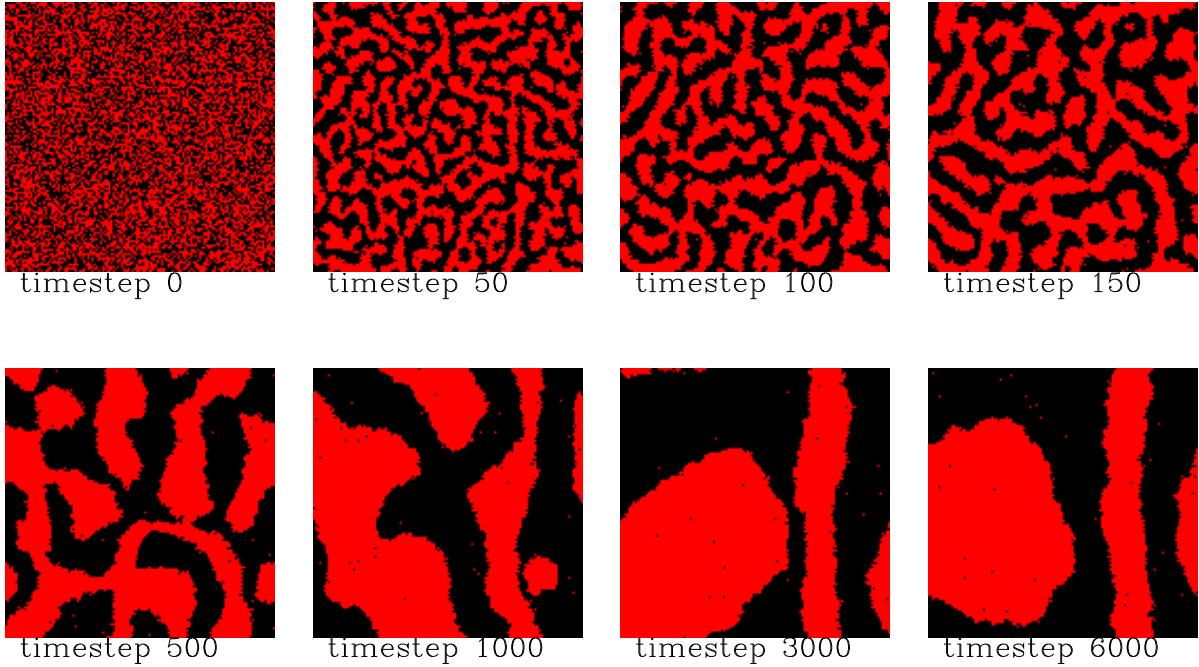
FIG. 4. *Nonequilibrium behaviour of a two-immiscible-fluid lattice gas, consisting of snapshots of the evolving two dimensional system taken at the timesteps shown.*

To make a detailed comparison between the immiscible oil-water fluid behaviour shown here and later simulations in which we introduce surfactant to the system, we make use of *circularly averaged structure functions*. We first calculate (Roland & Grant 1989) the two-dimensional structure factor of the colour charge, $s(\mathbf{k}, t)$,

$$s(\mathbf{k}, t) = \left\langle \frac{1}{N} \left| \sum_{\mathbf{x}} (q(\mathbf{x}) - q^{av}) e^{i\mathbf{k}\cdot\mathbf{x}} \right|^2 \right\rangle,$$

where $\mathbf{k} = (2\pi/L)(m\mathbf{i} + n\mathbf{j})$, $m, n = 1, 2, ..., L$, q($\mathbf{x}$) is the total colour charge at a site, q^{av} is the average value of the colour charge, L is the length of the system and $N = L^2$ is the number of sites in the system. The circularly averaged structure factor, which is what we actually evaluate numerically, is given by

$$S(k, t) = \frac{\sum_{\hat{k}} s(\mathbf{k}, t)}{\sum_{\hat{k}} 1}, \tag{35}$$

where $k = 2\pi n/L, n = 0, 1, 2, ..., L$, and the sum $\sum_{\hat{k}}$ is over a spherical shell defined by $(n - \frac{1}{2}) \leq \frac{|\mathbf{k}|L}{2\pi} < (n+\frac{1}{2})$. Note that the resolution of $S(k, t)$ depends on k_c, the cutoff frequency associated with the lattice, that is, for a real-space sampling interval of Δ the cut-off frequency is $1/2\Delta$; above this value of the frequency there is only spurious information carried as a result of aliasing. In our case, $k_c = (2\pi/L)n_c$, where we have chosen n_c to be the maximum possible value, which is half the lattice size. Figure 5 contains the temporal evolution of $S(k, t)$ for the case of two immiscible fluids. The data is averaged over five independent simulations. As time increases, the peak of $S(k, t)$ shifts to smaller wave numbers and its peak height increases. This behaviour is indicative of coarsening and will be used as a comparison for the surfactant-based systems described below.
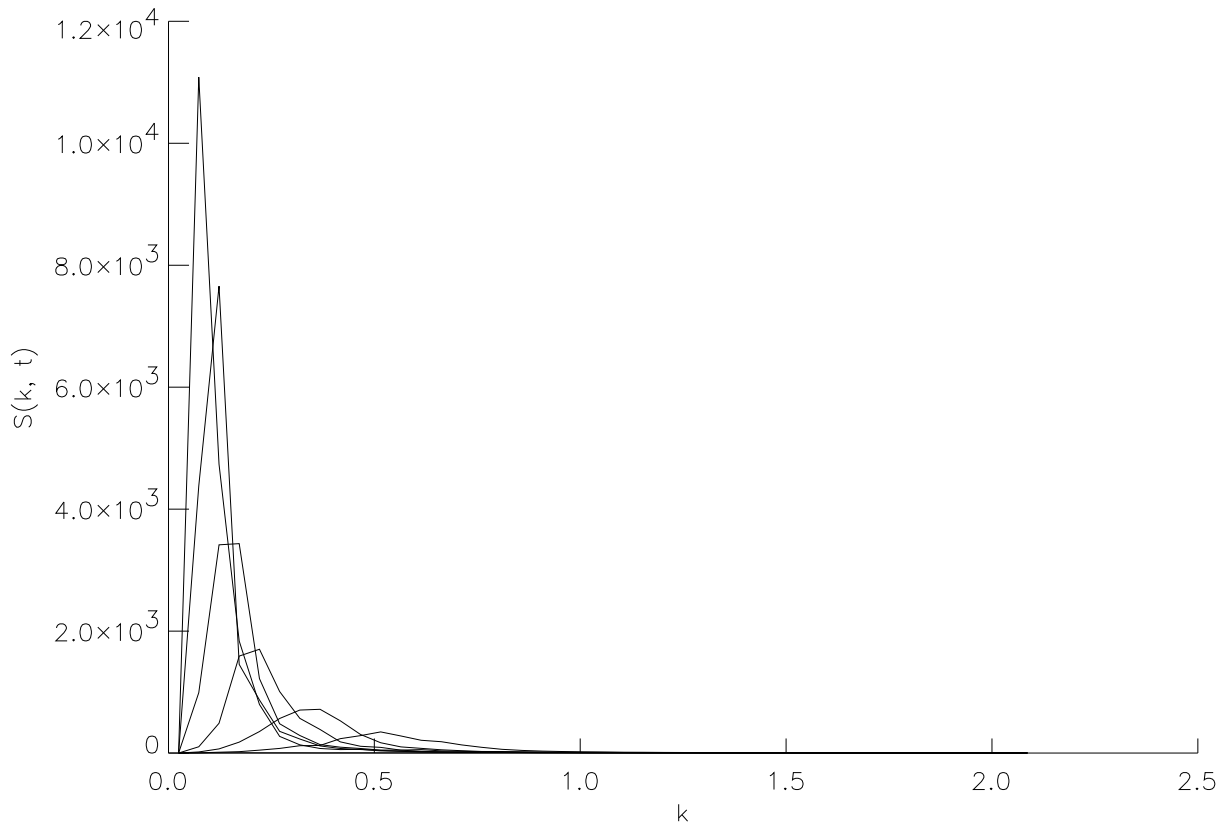
FIG. 5. *Temporal evolution of $S(k,t)$. Timesteps shown are, from bottom to top, t = 0, 80, 200, 400, 800, 1400, 2000.*

With sufficient averaging and a rescaling of variables it can be shown (Frisch *et. al.* 1986) that the Navier-Stokes equations for an incompressible fluid are obeyed within homogeneous regions of each of the fluids. (There are known problems with galilean invariance due to a spurious factor in front of the inertial term. This issue is discussed later in this paper.) It is also possible to show, as a result of the formation of interfaces, that physically realistic interfacial tensions exist. In terms of the basic two-species immiscible lattice-gas, surface tension has been studied from both a theoretical and a numerical viewpoint in a recent paper by Adler, d'Humières and Rothman (Adler *et. al.* 1994). Using a bubble experiment as described in their paper, we can investigate the validity of our basic model by evaluating the surface tension in the immiscible fluid case, noting that the measurement of surface tension requires the presence of an interface between two *macroscopically* defined phases. We use Laplace's law, which in two dimensions is

$$P_{\text{in}} - P_{\text{out}} = \frac{\sigma}{R},$$

where R is the radius of the bubble, P_{in} is the average pressure within the bubble and P_{out} the average pressure outside. The results from simulations are shown in Fig. 6. They give good agreement with Laplace's law, and a best-fitting line through the origin results in an estimate of $\sigma \approx 0.378$. This is close to the results given by Adler and co-workers, although we have done significantly less averaging than in their cited paper.
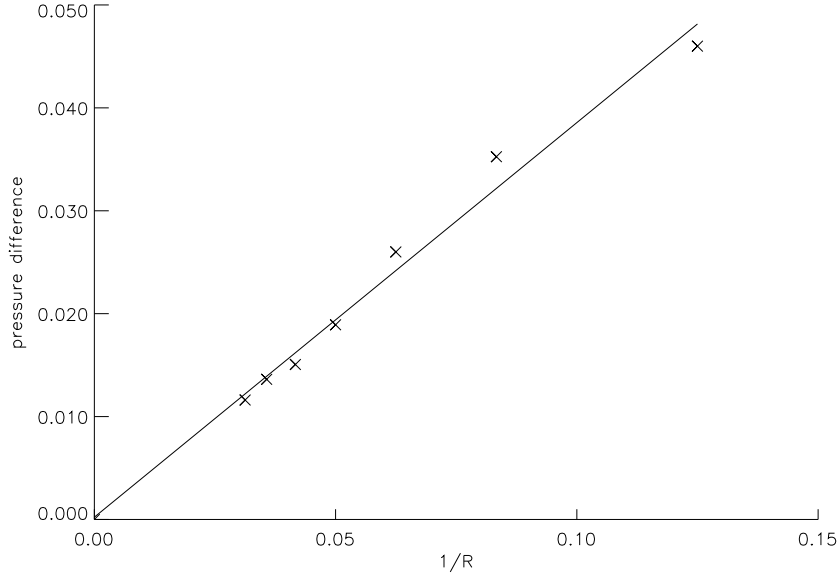
20

FIG. 6. *Verification of Laplace's law and estimation of surface tension*

D. Oil-Water-Surfactant Systems

Next we seek microemulsion-like behavior in ternary mixtures. We note that the introduction of the surfactant will cause all four of the terms in Eq. (33) to contribute in some way to the interaction energies of the collision process. In order that these terms enable us to reproduce basic microemulsion behaviour, we consider briefly what the physical contributions of the dipoles ought to be:

1. In real microemulsions, the surfactant molecules strongly prefer to sit with their hydrophilic heads in water and their hydrophobic tails in oil. Since the $\epsilon \Delta H_{dc}$ term in Eq. (33) arises as a result of the interaction of outgoing dipoles with the surrounding colour field, it is evident that we will want to include a large contribution from this term as it will favour vector dipoles aligning across, and sitting as near as possible to, oil-water interfaces, across which the colour field gradients are at their greatest.

2. The term $\mu \Delta H_{cd}$ in Eq. (33) results from the effect of surrounding dipoles on outgoing coloured particles. Since this will encourage the bending of dipoles around a central colour charge it may be important when it comes to looking at o/w and w/o microemulsion droplet phases, but a careful balance will have to be struck between this and the $\epsilon \Delta H_{dc}$ term to stop it from destroying the overwhelming tendency for surfactant to sit at oil-water interfaces, especially when we are looking to observe bicontinuous structures.

3. The final term $\zeta \Delta H_{dd}$ in Eq. (33) arises as a result of the interactions between dipoles, and will allow attraction or repulsion to take place depending on the sign of ζ. This term may be of limited use for modelling more general amphiphile-containing systems because, at present, our model does not differentiate between the relative strengths of the hydrophobic and hydrophilic interactions in amphiphile molecules.

After this assessment of the relative values of these constants, including

- the need for ϵ to be relatively large when compared with the other constants (see point 1. above),

- the realisation that an effective useful maximum value for ϵ exists, due to constraints imposed by the calculation of modified Bessel functions in the collision update process (see Section IV H),

21

- the need to compare our results with the known basic lattice-gas behaviour, suggesting that initially we maintain the value of α used in the two-immiscible-fluid case,

- some simulation work,

we arrived at the following set of coupling constants, that should allow us to model the various experimentally observed microemulsion characteristics :

$$\alpha = 1.0, \mu = 0.05, \epsilon = 8.0, \zeta = 0.5. \tag{36}$$

We use this as a 'canonical' set of coupling constants in the remainder of this paper.

E. Binary phases: From monomers to micelles

If one adds a small amount of amphiphile to water, then those surfactant molecules, while being highly dynamic within the bulk water phase, will remain distinct from one another and exist as *monomers*. Gradually increasing the amount of amphiphile in the system just increases the density of these monomers until, at the critical micelle concentration, the monomers begin to form micelles. These give the system characteristic structure and should be discernible in our simulations. The micelles themselves are dynamic objects and are not necessarily very long lived, since individual molecules are free to detach themselves, meet with other monomers and/or micelles and rejoin to form new structures; the kinetics of simple micelle formation can be modelled on the basis of a Becker-Döring theory (Coveney & Wattis 1995). Individual micelles do not grow without limit; if more surfactant is added to the system it will form new micelles rather than increasing the size of those already present. This is because, energetically, only a certain number of amphiphile molecules are able to fit around one central point to produce a micelle structure (for real micelles, the characteristic number of monomers contained within a micelle depends on the details of the surfactant's molecular structure). Consequently we do not expect to see evidence of micelles coalescing and growing in an unbounded manner in our simulations.
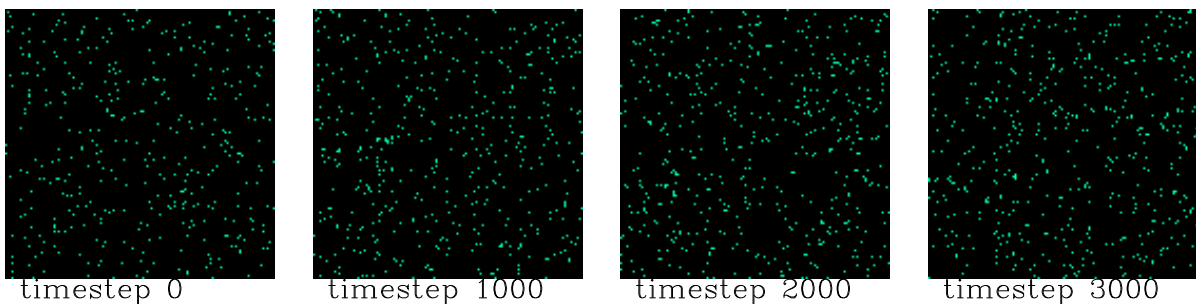

timestep 0   timestep 1000   timestep 2000   timestep 3000

FIG. 7. *Time evolution of binary water - surfactant phase, for the case with surfactant - water ratio 1:8.*

timestep 0   timestep 1000   timestep 2000   timestep 3000
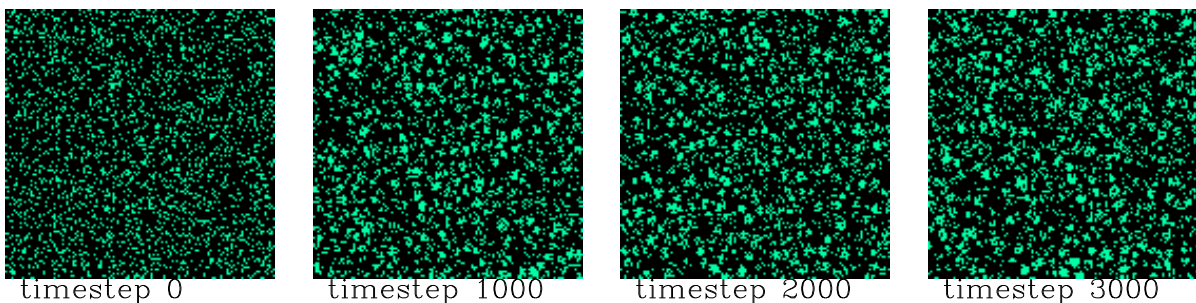
FIG. 8. *Time evolution of binary water - surfactant phase, for the case with surfactant - water ratio 1:2.*

We performed two simulations, one with a low concentration of surfactant and the other with a concentration exceeding the critical micelle concentration of the system. In both cases, the initial condition consists of placing water and surfactant particles on the lattice randomly. The visual results of the simulations are shown below. Due to the limitations of the visualization technique employed, we require further proof of the existence of structure and so perform a more quantitative analysis by calculating circularly averaged structure functions of the surfactant density (Kawakatsu *et. al* (1993)). For consistency, the coupling constants used in both simulations are as defined in Eq. (36). Figure 7 shows the result of a system containing a surfactant-to-water ratio of 1:8, equivalent to a initial reduced density of 0.4 for water and 0.05 for surfactant. As before a majority rule is employed to display the type of particle present at each site.
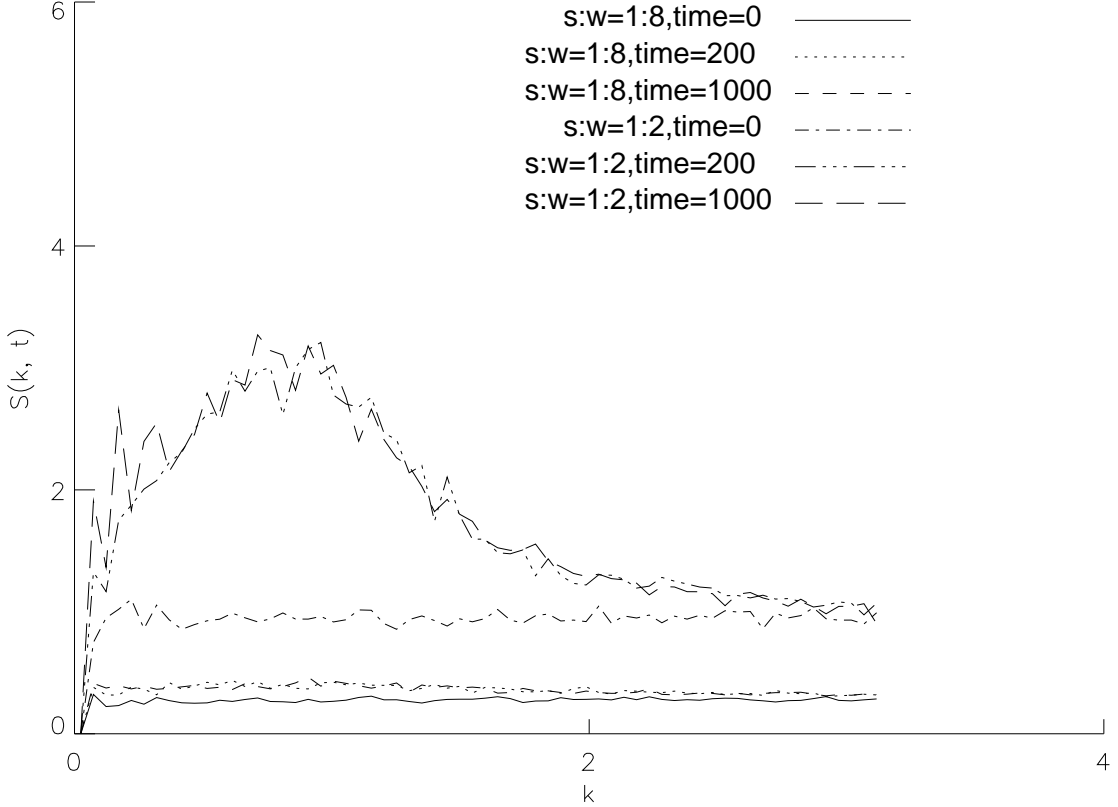
FIG. 9. *Temporal evolution of surfactant density $S(k, t)$ for binary water and surfactant mixtures.*

As can be seen in Fig. 7, with low surfactant concentration there is very little aggregation of the monomers throughout the simulation. This is backed up by the structure factor calculations, shown in Fig. 9, which indicate no structure formation during the timescale of the run. In stark contrast, Fig. 8, which has a surfactant-water ratio of 1:2, initial reduced density 0.4 for water and 0.2 surfactant, clearly indicates the formation of small, structured objects, along with the presence of some monomers. These structured objects are indeed micelles; they appear in the early stages of the simulation and, although being highly dynamic, do seem to maintain their size and shape. This analysis is confirmed by the circularly averaged structure factors shown in Fig. 9, where an average taken over ten independent runs is displayed. The graph clearly indicates the formation of structure when the surfactant-to-water ratio is 1:2, and an absence of structure when the ratio is 1:8.
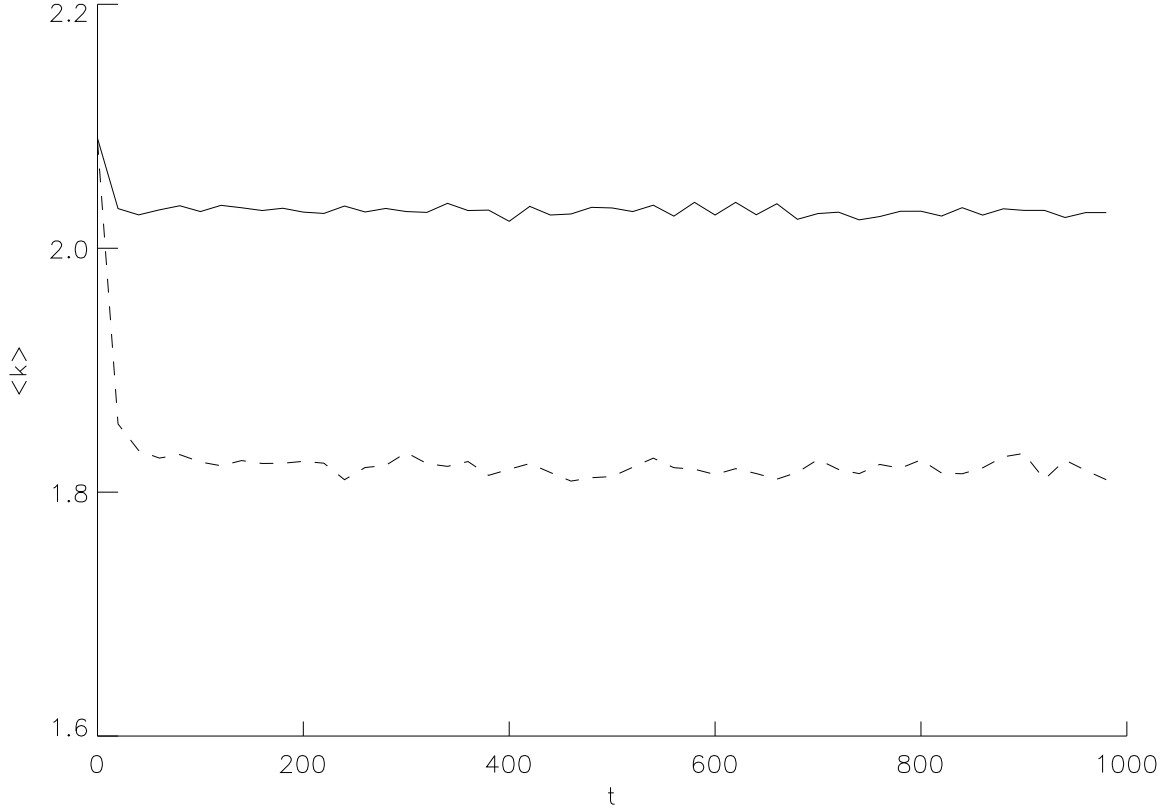
FIG. 10. *Characteristic wave number* $\langle k(t) \rangle$ *against time t. The unbroken line on the graph corresponds to the case with surfactant - water ratio 1:8 and the broken line to the ratio 1:2.*

The fact that the plots at times 200 and 1000 are virtually identical suggests that the characteristic sizes of the micelle-like structures saturate at early times during the simulation and that they do not change dramatically thereafter. Thus, as expected, the structures do not grow without limit.

This is made still more clear by Fig. 10, in which we plot the temporal evolution of the characteristic wave number,

$$\langle k(t) \rangle = \frac{\sum_{k=0}^{k_c} k S(k, t)}{\sum_{k=0}^{k_c} S(k, t)},$$

the inverse of which is a measure of the average domain size (Kawakatsu *et. al* 1993).

We see that, in contrast to the case of low amphiphile concentration, we get initial growth of the surfactant domains which very rapidly levels off to some constant size.

F. Ternary phases: lamellae

We first investigate the stability of a lamellar structure, which is composed of alternating layers of oil-rich and water-rich phases separated by surfactant molecules. We look at the system with and without surfactant present in order for a critical comparison to be made. In a similar way to Kawakatsu & Kawasaki (1990) we set up the initial configuration of the system, resulting in layers of oil and water eight sites wide, all sites having a reduced density of 0.5. It is clear that if our model is exhibiting the correct behaviour, then we

24

would expect there to be a critical density of surfactant required at the oil-water interfaces in order for the layered structure to be stable. Consequently, we set up a simulation where there is a layer of surfactant at each of the oil-water interfaces that is just a single site wide, but with a reduced density on these amphiphilic sites equal to 0.8. The results of the simulations undertaken are shown in Fig. 11, Fig. 12 and Fig. 13 below. Figure 11 is the pure oil-water case with $\alpha = 1.0$, ensuring that the oil and water particles will want to act as immiscible fluids and so we expect to see phase separation evolving from the layered initial condition. Figure 12 has surfactant present as described above but with coefficients $\alpha = 1.0, \mu = 0.0, \epsilon = 0.0, \zeta = 0.0$, while Fig. 13 has a similar amount of surfactant in the system but in this case the coefficients are as defined by Eq. (36), and so the full set of interaction terms in our model are now included. Note that we let the last two simulations evolve to late times in order to check that we are not just observing metastable states with long equilibration times which might arise as a result of the particular set of initial conditions chosen.
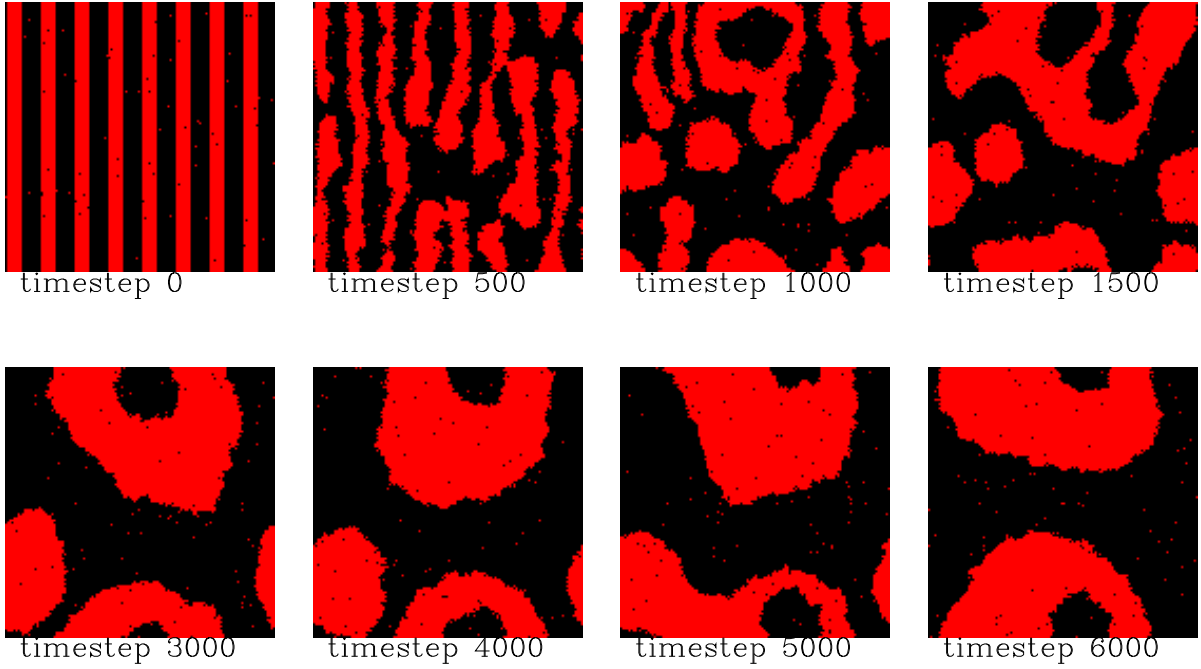

FIG. 11. *Time evolution from initial lamellar configuration, for the case without surfactant.*

The probabilistic, dynamical nature of our model means that there are sufficient fluctuations present to enable oil and water particles from the initially separated layers to move locally, and in so doing come under the influence of the colour field gradients produced by other layers of the same type. Since $\alpha = \beta = 1.0$, there is an inherent tendency for the oil and water to act as immiscible fluids and phase separate (*cf.*, Fig. 4), and that is exactly what the simulation, Fig. 11, reflects.
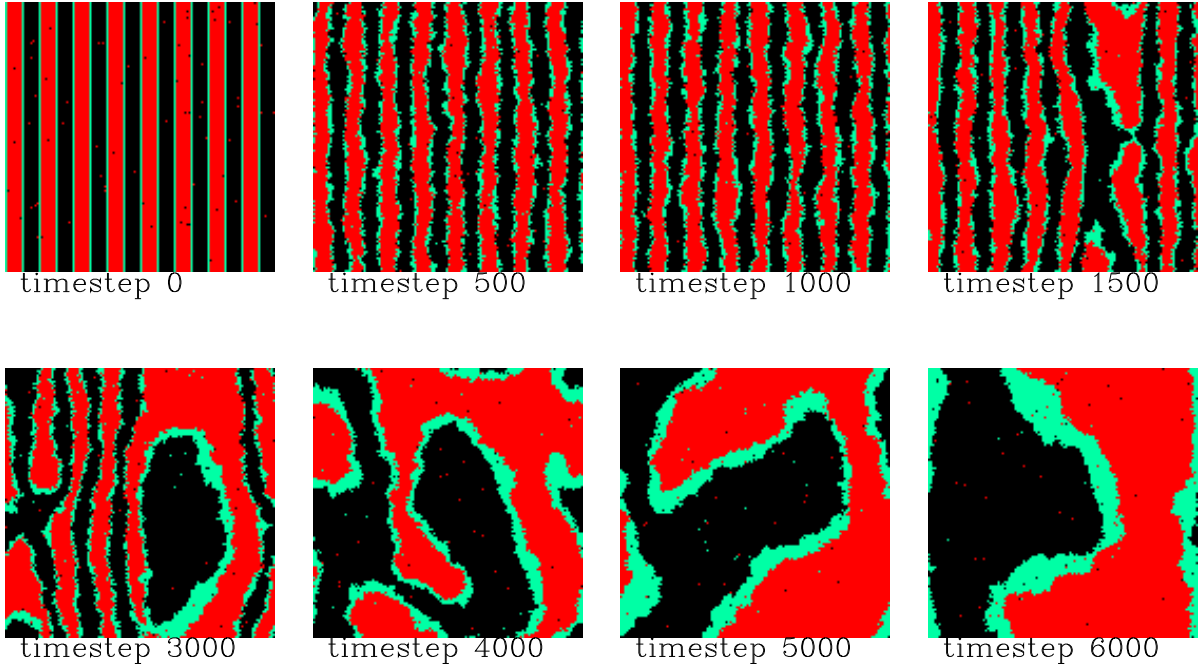
FIG. 12. *Time evolution from initial lamellar configuration, for the case with surfactant but only α non-zero.*
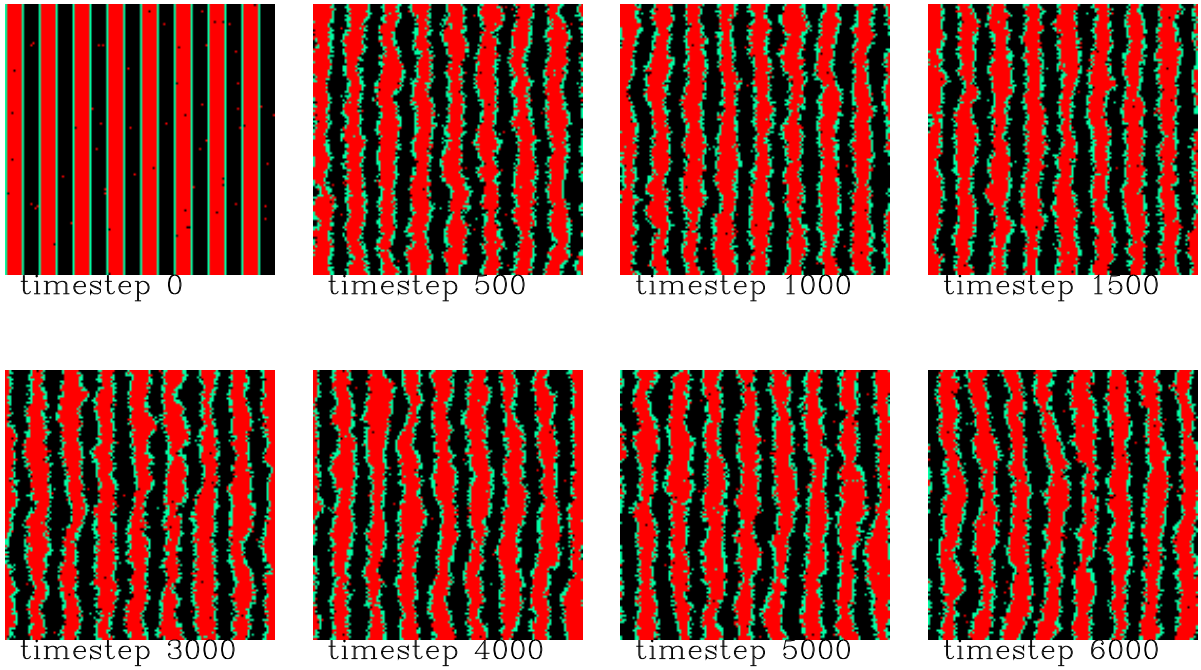

FIG. 13. *Time evolution from initial lamellar configuration, for the case with surfactant and coefficients set as* $\alpha = 1.0, \mu = 0.05, \epsilon = 8.0, \zeta = 0.5$.

The second result, displayed in Fig. 12, is included as a control. It shows that the mere presence of a third type of particle at the oil-water interfaces is not enough to artificially stabilise the structure of the layers. However it is clear that the initial breakup of the layers takes place at a later time than for the case of two species only (Fig. 11). This is because of the presence of a third species between the oil and water layers, meaning that on average the oil/water particles will have further to move before they can come under the influence of a colour field set up by a neighbouring layer of like colour. An interesting point to observe here is the forced accumulation of the third species, in thick layers at the interfaces, once the oil and water begin to act as immiscible fluids and phase separate.

Finally we come to Fig. 13. The presence of the colour dipoles and the fact that their corresponding interaction terms can affect the collision outcomes means, as the simulation clearly shows, that it is now energetically favourable for the surfactant to remain at oil-water interfaces. In spite of the fact that the dipolar vectors that represent the surfactant molecules are initially assigned random angles between 0 and 2π, so that again we have initial fluctuations in the system, it is clear that the integrity of the lamellar structure is maintained and appears to be completely stable, even at late times in the simulation. At the oil-water interfaces the amphiphile sits in *thin* layers (*cf.* Fig. 12), which compares well with the knowledge that in real microemulsions amphiphile tends to reside in monolayers between regions of oil and water. The greater the surface tension that exists at the interfaces within a system, the more that system will act to try and reduce the amount of interfacial area present. Since in our model the presence of surfactant at the oil/water interfaces results in stabilisation of the lamellar structure, and such a structure has a large interfacial area, it appears that the surface tension is indeed being reduced. This analysis and result provide initial confirmation of microemulsion-like behaviour in our model.

G. Ternary phases: Oil-in-water (water-in-oil) and bicontinuous microemulsions

Finally we use our model to simulate the different ternary *microemulsion phases* that are possible in $2D$, namely, the oil-in-water droplet and the bicontinuous phases. (Note that since, at present, our model treats oil and water molecules in symmetric fashion, the oil-in-water phase could equally well represent a water-in-oil phase.) In reality the two distinct microemulsion phases will form if there are the correct relative amounts of oil, water and surfactant in the system at a given temperature. The oil-in-water droplet phase typically consists of finely divided, spherical regions of oil, with stabilising monolayers of surfactant surrounding them, sitting in the bulk water background. If one increases the relative amount of oil in the system and there is sufficient amphiphile present, one will observe the formation of mutually percolating tubular regions of oil and water, with layers of surfactant sitting at the interfaces. In both these cases, the equilibrium state does not correspond to complete separation of the immiscible oil and water regions, but rather to complex structures with very different characteristic length scales that form as a result of the presence of amphiphile.

In order to reproduce the oil-in-water phase, we set up a simulation with a random initial configuration consisting of a $3 : 1.9 : 0.7$ water-to-surfactant-to-oil ratio, respectively, with an averaged reduced density of 0.56. To maintain consistency between our various simulations, we again use the coupling constants as defined in Eq. (36). Figure 14 displays the result. We see the rapid formation of many oil-in-water droplets, whose size increases slightly, but not without limit. This is representative of the experimental microemulsion state and occurs because the layer of surfactant that surrounds the droplets acts to stabilise the interfaces and thereby inhibits the further flow of oil to the centre of any such droplet, as well as discouraging their coalescence.
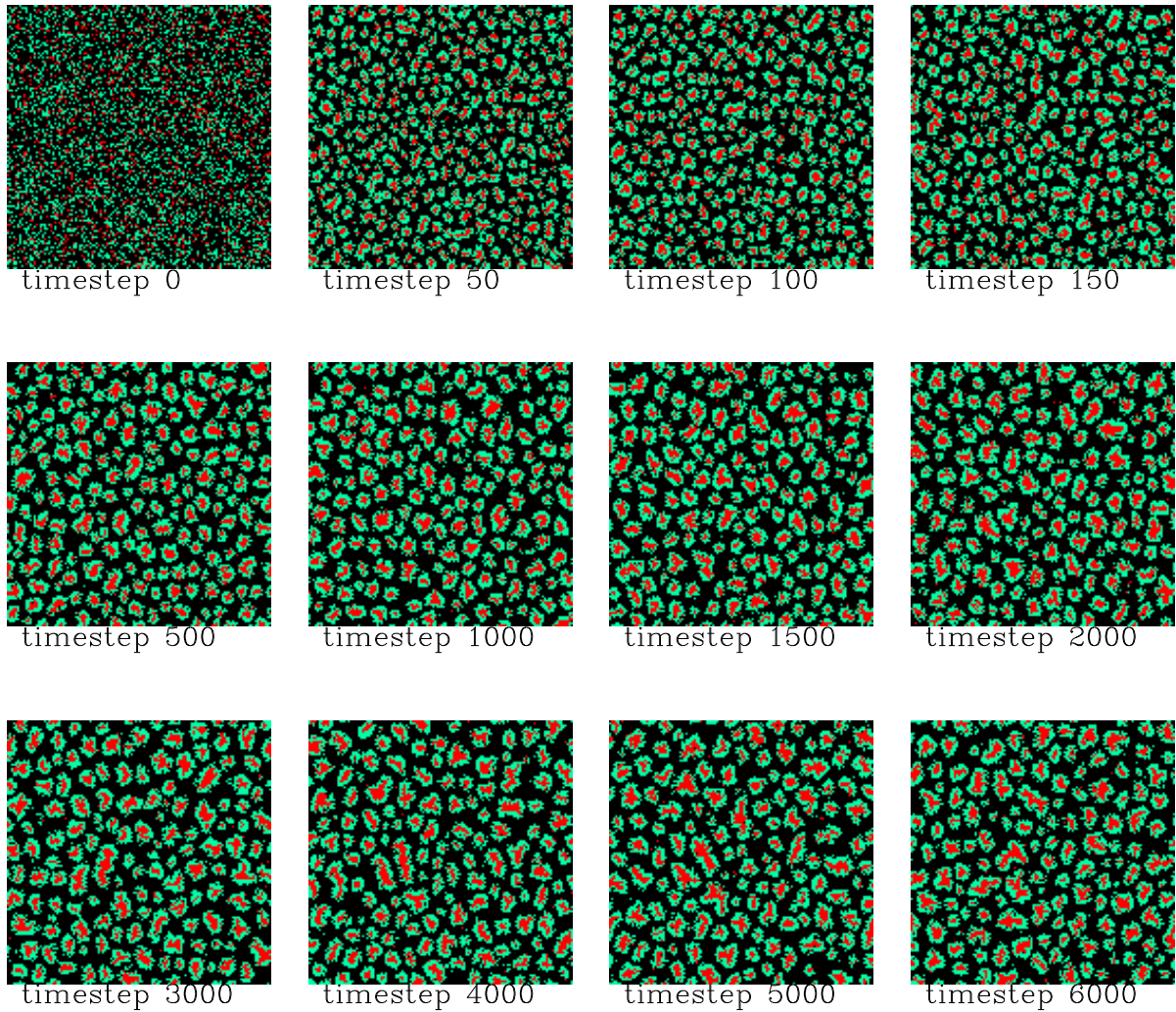
FIG. 14. *Time evolution of oil-in-water microemulsion phase.*

In order to quantify this result, we calculate the circularly averaged structure factor of the colour charge, and plot the result in Fig. 15. We observe the early-time growth of the peak height of $S(k,t)$ as the peak itself shifts towards lower values of the wavelength, indicating that the droplets form and grow to some characteristic size. From at least timestep 800 onwards there appears to be a negligible amount of further growth or movement of the position of the peak, indicating that the droplets have reached their maximum size and will grow no more. This simple analysis confirms the ability of our model to attain a microemulsion droplet phase within a certain region of the overall phase diagram.
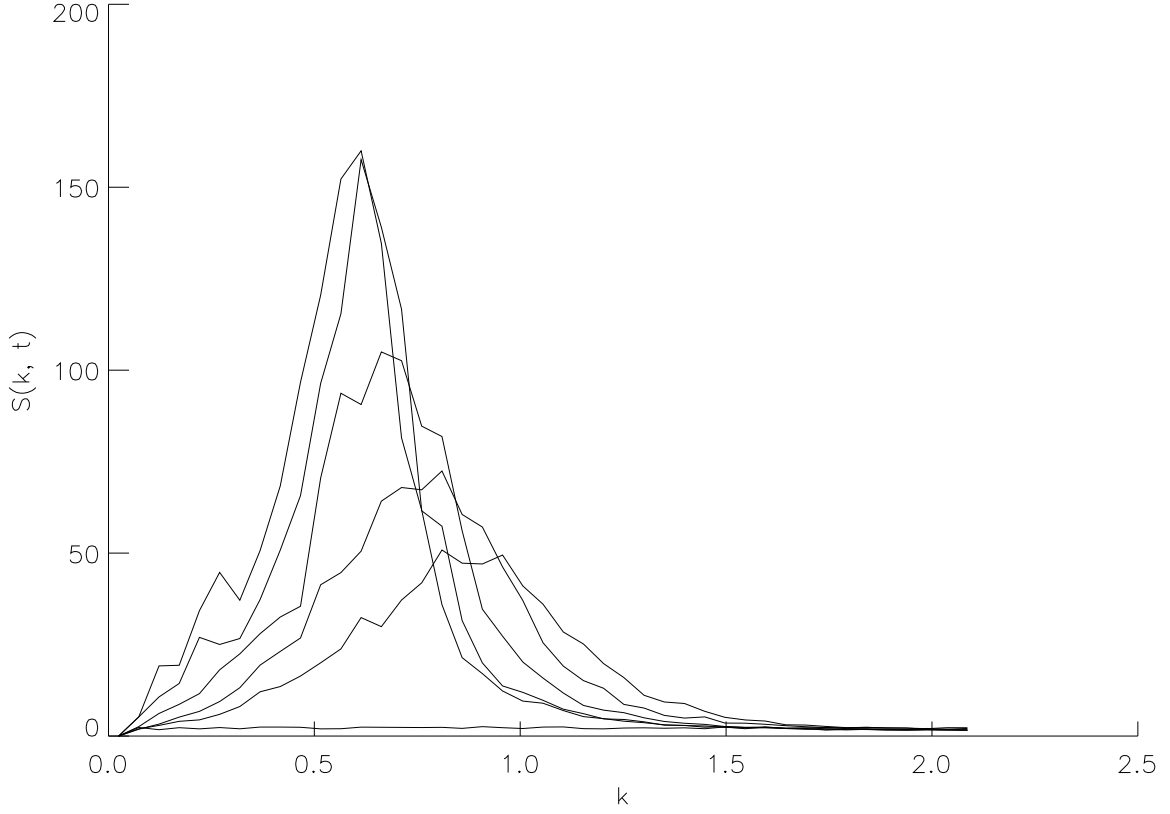
FIG. 15. *Temporal evolution of $S(k,t)$ for microemulsion droplet case. Timesteps shown are, from bottom to top,* $t = 0, 40, 80, 200, 800, 2000.$

To demonstrate the existence of the bicontinuous regime within the model's phase diagram, we use the same coupling constants as before but simply increase the relative amount of oil present in the system. Hence this second simulation, shown in Fig. 16, has a random initial mixture with a reduced density 0.55 and a $3 : 2.25 : 3$ oil-to-surfactant-to-water ratio.
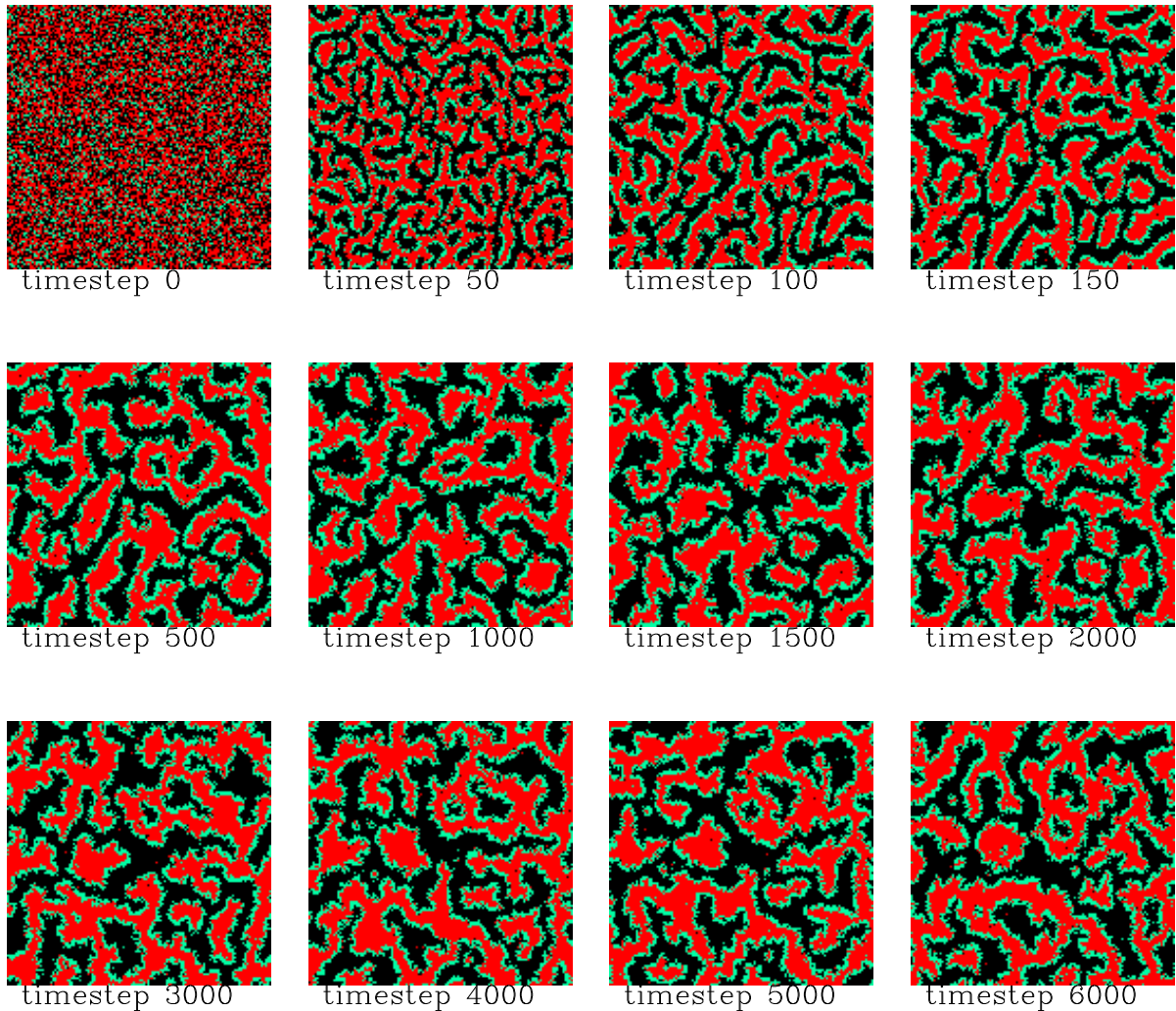
FIG. 16. *Time evolution of bicontinuous microemulsion phase.*

We observe the growth of an interconnected network of tubular-like regions of oil and water, separated by *thin* layers of amphiphile that ensure the stabilisation (reduction of oil-water surface tension) of the bicontinuous régime, together with the formation of droplets and some micelle-like objects. Note that on average the width of the oil and water regions grows in size up to about 500 timesteps, during which time the surfactant particles migrate around the various oil-water interfaces so as to spread themselves uniformly. Beyond this stage the system changes very little, indicating that the observed bicontinuous phase, although always slightly affected by the underlying lattice gas dynamics, is stable. To appreciate the significance of this result, the snapshots and timescale should be compared with the two-immiscible-fluid case (Fig. 4), the only difference between the two being the introduction of amphiphile and the accompanying interaction terms.

To permit further analysis of this result, we calculate the circularly averaged structure factor of the colour charge, in an exactly analagous way to that for the immiscible fluid case. The result we obtain is shown in Fig. 17, which is an average over five independent simulations.
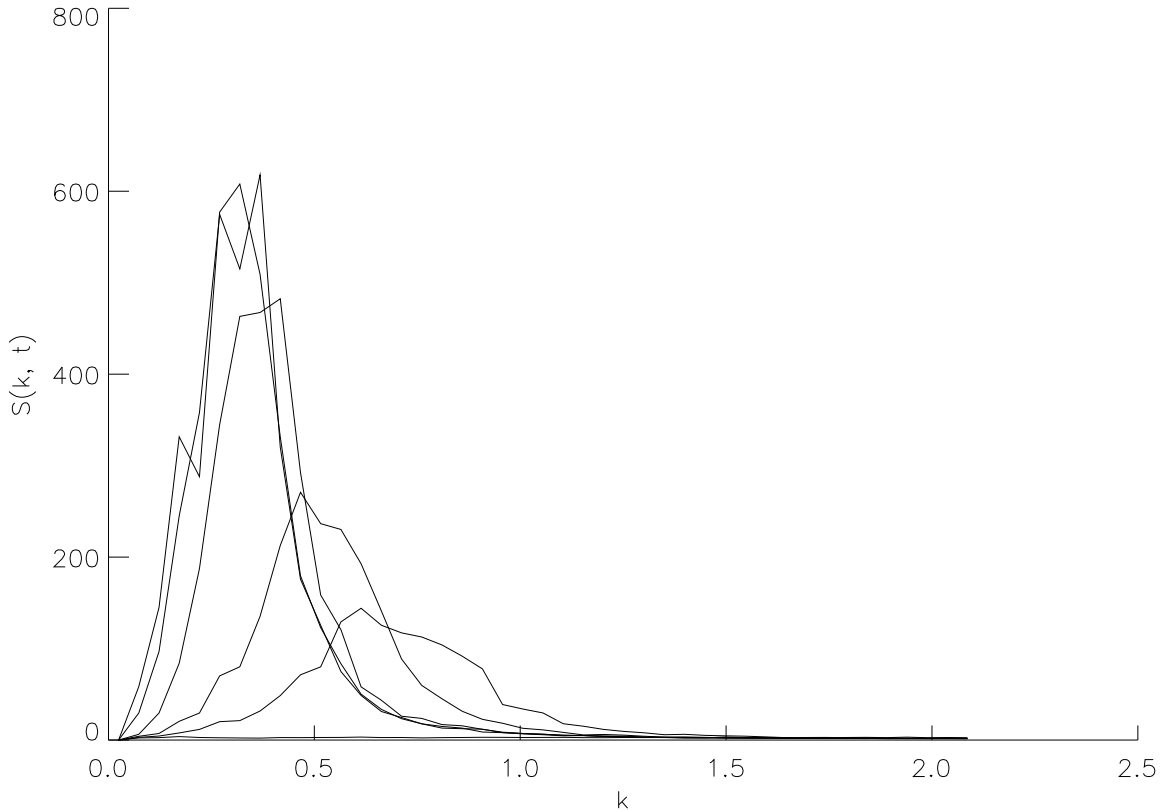
30

FIG. 17. *Temporal evolution of* $S(k,t)$ *for bicontinuous microemulsion case. Timesteps shown are, from bottom to top,* $t = 0, 40, 80, 200, 800, 2000.$

Comparing this with Fig. 5, which shows the structure factor for the immiscible oil and water case, we see that after about 200 timesteps the growth of the peak of the structure factor is dramatically slowed down by the presence of the surfactant, and also that some minimum k is reached below which the location of the peak no longer shifts, indicating that the underlying immiscible fluid coalescence process has been inhibited owing to the presence of the amphiphile.

VI. DISCUSSION

The results described above provide evidence of the ability of our model to reproduce the fundamental equilibrium microemulsion phases. Since the dynamics conserves momentum in addition to mass, we expect that it ought to be able to model dynamic, nonequilibrium behavior as well. In drawing this conclusion, however, an important caveat should be mentioned: as noted earlier, lattice gases can break galilean invariance, due to the presence of a preferred galilean frame of reference, namely the lattice itself. Mathematically, this problem manifests itself by a spurious factor multiplying the inertial term in the momentum-conserving Navier-Stokes equation. For a single-phase lattice gas, this factor can easily be scaled away; for compressible flow, or for multiphase flow with interfaces, however, the presence of this factor is problematic, and various techniques have been proposed to remove it. It has been shown that this can be done at the expense of complicating the collision rules by introducing judicious violations of semi-detailed balance (d'Humières *et. al.* 1987), by adding many rest particles at each site (Gunstensen & Rothman 1991b), or by using multiple bits in each direction rather than only one (Boghosian *et. al.* 1995). In the present paper, we have evaded

31

this issue by focusing only on equilibrium phenomenology, or on creep flow situations for which the inertial term is negligible. For flow at finite Reynolds number, however, this issue must be addressed using one of the above-mentioned methods, and we plan to do this in future work.

In spite of this limitation, we note that the model exhibits some interesting effects. One of these, the roughening of the interface, is evident in Fig. 16. The surfactant, in its attempt to increase the surface area surrounding a given volume of oil, has caused the creation of a fractal, fluctuating interface. Lattice gases have already been used as a tool for studying interface fluctuations in immiscible fluids (Adler *et. al.* 1994), we now have the ability to extend these studies to include the effect of surfactant on the interface.

VII. CONCLUSIONS

We have developed a model for momentum-conserving simulations of the dynamics of microemulsions and other related self-assembling amphiphilic systems. Using an electrostatic analogy for both the colour particles and the amphiphilic colour dipoles we have been able to derive the various energy interaction terms, including that of the Rothman-Keller immiscible fluid lattice gas, from a microscopic particulate viewpoint. Using a single set of coupling constants, we have shown that our model exhibits the correct $2D$ phenomenology for both binary and ternary phase systems using a combination of visual and analytic techniques; various experimentally observed self-assembling structures form in a consistent manner as a result of adjusting the relative amounts of oil, water and amphiphile in the system. The presence of enough surfactant in the system clearly halts the phase separation of oil and water, and this is acheived without altering the coupling constant α from a value that produces immisible behaviour in the case of no surfactant. In achieving these results, we have also demonstrated for the first time that lattice gases may be used to investigate the dynamics of fluids with very complex interactions.

Consequently we should be able to investigate a plethora of microemulsion-related problems, including, for example, roughening and interface fluctuations in microemulsions, and the behaviour of microemulsions under flow conditions. Such studies are fairly easily implemented using lattice gases, and should also permit us to observe the various microemulsion phases flowing through complex geometries such as porous media. Future extensions include a $3D$ version of our model, which would allow various applications in many different areas of science to be investigated.

ACKNOWLEDGMENTS

APPENDIX A: DERIVATION OF EQUIVALENCE CLASSES

As discussed in the main text, the partitioning of the $(M+1)^n$ possible states, in which each lattice site can exist, into equivalence classes of states that have the same values for the $(M+D)$ conserved quantities is required for the specification of the collision process. Here we show how to derive those equivalence classes for lattice collisions conserving both mass and momentum. We deal specifically with the case of three species ($M = 3$) on a two-dimensional lattice ($D = 2$) so that we conserve three masses and two components of momentum.

Since we have seven lattice vectors per site (six plus the rest particle) and each of these directions is assigned two bits, there is a total of $n = 14$ bits per lattice site and hence 2^{14} possible states per site. Note that the two bits correspond to no molecule (00), a water molecule (01), a surfactant molecule (10), and an

oil molecule (11). We also need a way to identify the classes. We tag them by the number of oil, water and surfactant particles, the x-momentum and the y-momentum. Since there is a maximum of seven particles of any type at a lattice site the masses can be stored using three bits for each, while the x and y components of the momentum will need four bits and three bits respectively as discussed below, giving a total of sixteen bits of class information.

To see why the momentum components require four and three bits, respectively, we orientate the hexagonal lattice so that the lattice vectors are

$$\hat{\mathbf{c}}_j = \begin{cases} \hat{\mathbf{x}}\cos\left(\frac{2\pi j}{6}\right) + \hat{\mathbf{y}}\sin\left(\frac{2\pi j}{6}\right) & \text{for } 0 \leq j \leq 5 \\ \mathbf{0} & \text{for } j = 6. \end{cases}$$

Defining $n_i \equiv \sum_\alpha n_i^\alpha$, the x-momentum is given by,

$$p_x = n_0 + \frac{1}{2}n_1 - \frac{1}{2}n_2 - n_3 - \frac{1}{2}n_4 + \frac{1}{2}n_5.$$

Since this can be a non-integer we multiply it by two to get a unique integer identifier for p_x,

$$2p_x = 2n_0 + n_1 - n_2 - 2n_3 - n_4 + n_5. \tag{A1}$$

We observe that this can be negative and that we would like an unsigned integer to identify the x-momentum, so we make use of the fact that N,

$$N = n_0 + n_1 + n_2 + n_3 + n_4 + n_5 + n_6,$$

is a conserved quantity, since it is just the total number of particles at a site. We then add twice N to Eq. (A1) for p_x to get,

$$2\left(N + p_x\right) = 4n_0 + 3n_1 + n_2 + n_4 + 3n_5 + 2n_6,$$

which we can now use as an identifier for the x-momentum. Note that its maximum value is 14, so we need four bits to store this quantity.

Similarly the y-momentum is given by

$$p_y = \frac{\sqrt{3}}{2}(n_1 + n_2 - n_4 - n_5).$$

In a similar way to that just described we multiply this equation by $2/\sqrt{3}$ and add N, getting a unique y-momentum identifier,

$$\left(N + \frac{2}{\sqrt{3}}p_y\right) = n_0 + 2n_1 + 2n_2 + n_3 + n_6.$$

This has a maximum value of 7, so it can be stored in only 3 bits.

We can now loop through all states and obtain the 16-bit class identifier for each one. These class identifiers are then sorted so that states in the same equivalence class are next to each other. The states and class identifiers can subsequently be separated into two corresponding arrays. We use the 14-bit state as a key to look up the initial index and length of that state's equivalence class. All three look-up tables, the class-pointers, class-lengths and states are then integer arrays of length 2^{14} which can be precomputed and easily read by the main program code at run time.

APPENDIX B: SAMPLING PROCEDURE

We can sample the outgoing occupation numbers $\mathbf{n}'$ directly from Eq. (31). This is accomplished by obtaining the total energy value for each outgoing state in the particular equivalence class, normalising these energies and then making use of a histogram probability distribution method to select the outgoing state.

Similarly, we sample the outgoing dipolar orientations from Eq. (32). Obtaining the outgoing angles from this, however, is not straightforward; we need to sample this function but can not do it exactly as in the case of the outgoing occupation numbers. The probability distribution for each dipolar angle θ_i'', for $i = 1, \cdots, n$, is given by

$$Q(\theta'') = \frac{\exp\left[-z\cos\theta''\right]}{2\pi I_0(z)},$$

where $z = \beta n_i^{S'} A_i(s)$ and $\theta'' = \theta_i' - \phi_i(s)$. This function is that shown in Fig. (18).
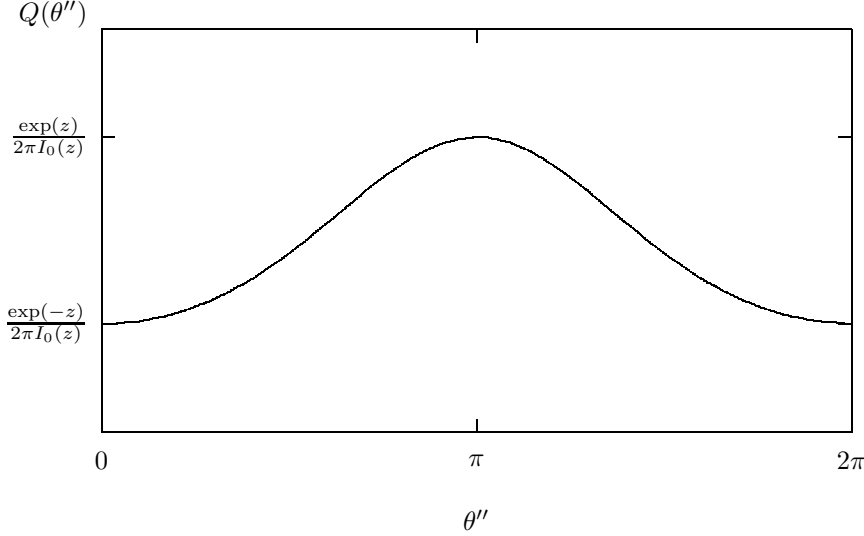

FIG. 18. *Probability Distribution* $Q(\theta'')$

For low z we use a rejection algorithm to sample from this function. This is done by choosing a random point, (θ, y), uniformly distributed in the rectangle of width 2π and height $e^z/(2\pi I_0(z))$. If the chosen point is below the curve $Q(\theta'')$ then it is accepted and the first coordinate of the point becomes the sampled θ''; if the point lies above the curve it is rejected and the procedure is repeated. One problem with this method is that the efficiency of the required algorithm goes as the ratio of the area under the curve to the area of the rectangle, so that it becomes inefficient for large z. It is, however, reliable up to at least $z = 6$. For larger values of z we need another technique. We observe that when z is large the distribution $Q(\theta'')$ is very peaked near $\theta'' = \pi$ and can hence be approximated as follows:

$$
\begin{aligned}
Q(\theta'') &= \frac{\exp\left[-z\cos\theta''\right]}{2\pi I_0(z)} \\
&= \frac{\exp\left[z\cos\left(\theta'' - \pi\right)\right]}{2\pi I_0(z)} \\
&\approx \frac{\exp\left[z\left(1 - \frac{1}{2}\left(\theta'' - \pi\right)^2\right)\right]}{\frac{2\pi}{\sqrt{2\pi z}}\exp(z)}
\end{aligned}
$$

where we have used a Taylor expansion about $(\theta'' - \pi)$ and the asymptotic expansion of $I_0(z)$. This gives us

$$Q(\theta'') = \sqrt{\frac{z}{2\pi}}\exp\left[-\frac{z}{2}\left(\theta'' - \pi\right)^2\right].$$

We observe that this is a normalised Gaussian in θ'', centered at π and of width $\sqrt{1/z}$, and consequently it is straightforward to sample θ'' from this using the $2D$ Box-Mueller algorithm.

34

APPENDIX: REFERENCES

Adler, C., d'Humières, D. & Rothman, D.H. 1994 *J. Phys. I (France)* **4**, 29-46.

Boghosian, B.M., Margolus, N.H. & Yepez, J. "Finite-Integer Lattice Gases," in preparation.

Cazabat, A.M., Langevin, D., Meunier, J. & Pouchelon, A. 1982 *Adv. Colloid Interface Sci.* **16**, 175-199.

Chan, C.K. & Liang, N.Y. 1990 *Europhys. Lett.* **13**, 495-500.

Coveney, P.V. & Wattis, J.D. "Analysis of a generalised Becker-Döring model of self-reproducing micelles," 1995 preprint.

Dawson, K.A. 1986 *Physical Review A.* **35**, 1766-1773.

Frisch, U., Hasslacher, B. & Pomeau, Y. 1986 *Phys. Rev. Lett* **56**, 1505-1508.

Gelbart, W.M., Roux, D. & Ben-Shaul, A. (eds) 1993 *Modern Ideas and Problems in Amphiphilic Science.* Berlin: Springer.

Gompper, G. & Schick, M. 1989 *Chem. Phys. Lett.* **163**, 475-479.

Gompper, G. & Schick, M. 1995 *Phase Transitions and Critical Phenomena* **16**, to be published.

Gunstensen, A.K. & Rothman, D.H. 1991a *Physica D.* **47**, 47-52.

Gunstensen, A.K. & Rothman, D.H. 1991b *Physica D.* **47**, 53-63.

Gunstensen, A.K., Rothman, D.H., Zaleski, S. & Zanetti, G. 1991 *Phys. Rev. A* **43**, 4320-4327.

Gunstensen, A.K. 1992 *Ph.D. Thesis* M.I.T.

d'Humières, D. & Lallemand, P. 1987 *Complex Systems* **1**, 633-647.

Kahlweit, M., Strey, R., Haase, D., Kuneida, H. & Schmeling, T. 1987 *J. Colloid Interface Sci.* **118**, 436.

Kawakatsu, T. & Kawasaki, K. 1990 *Physica A* **167**, 690-735.

Kawakatsu, T., Kawasaki, K., Furusaka, M., Okabayashi, H. & Kanaya, T. 1993 *J. Chem. Phys.* **99**, 8200-8217.

Matsen, M.W. & Sullivan, D.E. 1990 *Phys. Rev. A* **41**, 2021-2030.

Roland, C. & Grant, M. 1989 *Physical Review B.* **39**, 11971-11981.

Rothman, D.H. & Keller, J.M. 1988 *J. Stat. Phys.* **52**, 1119-1127.

Rothman, D.H. & Zaleski, S. 1994 *Reviews of Modern Physics* **66**, 1417-1475.

Schick, M. & Shih, W-H. 1987 *Phys. Rev. Lett.* **59**, 1205-1208.

Stockfish, T.P. & Wheeler, J.C. 1988, *J. Chem. Phys.* **92**, 3292-3301.

Widom, B. 1984 *J. Chem. Phys.* **88**, 6508-6514.

Widom, B. 1986 *J. Chem. Phys.* **84**, 6943-6954.

Widom, B. & Dawson, K.A. 1986 *Physica A.* **140**, 26-34.

Wolfram, S. 1986 *J. Stat. Phys.* **45**, 471-526.